Electronic Supplementary Information

Pillared MOFs: structure and ring opening polymerization of cyclic esters

Yi Gong,[a] Fei Chen,[a] Jethro Beamish-Cook,[a] Mark R. J.Elsegood,[b] Max Derbyshire,[b] Oliver Rowe,[c] and Carl Redshaw,*[a]

[a] Department of Chemistry, University of Hull, Hull, HU6 7RX, U.K.

[b] Chemistry Department, Loughborough University, Loughborough, Leicestershire, LE11 3TU, U.K.

[c] School of Chemistry, University of East Anglia, Norwich, NR4 7TJ, U.K.

Contents

Experimental

General

All reagents were purchased from Sigma-Aldrich and were used with no further purification. Solvents were purchased from Fisher Scientific. The electric balance (Sartorius Analytical A200s) was used to weight chemicals. The hydrothermal reactions take place in an oven (memmert UF 30PLUS). All samples were prepared for BET and ROP studies *via* solvent exchange, by immersion in chloroform for 2 days, during which time the solvent was replaced several times. Samples were activated prior to testing by heating to 120 °C for 12 h under dynamic vacuum. BET data was collected on surface area and porosity analyzer (Micromeritics® TriStar), all samples were degassed in 80 ℃ over 2 to 3 hours by sample degas system (FlowPrep 060). Infra-red data (Nujol mulls, KBr windows) were collected using a Nicolet Avatar 360 FT IR spectrometer. Elemental analyses were performed by the National Elemental Analysis service at London Metropolitan University. MALDI-TOF mass spectra (Wyatt Analytical Ltd, Colwyn Bay, UK) were obtained in both positive-linear (LP/-1) and reflectron (RP/-3) modes on a Bruker Autoflex Speed MALDI-TOF spectrometer and analysed with Bruker PolyTools and Strohalm mMass (v5.5.0) software. TGA results were recorded on a TA instruments 2950 TGA HR V5.3 thermogravimetric analyser under an inert (N_2) carrier flow from 30 to 600 °C with a scanning rate of 2 °C min^{-1}. Powder X-ray diffraction data was collected by PANalytical Empyrean Series 2 using an Empyrean powder diffractometer equipped with a copper X-ray tube. On a spectrometer (JEOL ECZ 400S), ^1H NMR spectra were acquired at 400.2 MHz room temperature. GPC results were obtained from Viscotek range (VE 3580 RI detector, VE 1122 solvent delivery system, VE 5111 injector valve bracket, 270 dual detector).

Visualization and Simulation

Figures 1, 3, 5, 7, 9, 11, 13, 15, 17, 19, 21 were generated using CYLview (version 1.0)[1]. Figures 2, 4, 6, 8, 10, 12, 14, 16, 18, 20, 22, 33-26 and Figure S33 were generated using Vesta (version 3.0)[2]. Simulated PXRD data were calculated using Mercury. The structures in figure S33 were optimized by Gaussian 09W (DFT, B3LYP, 6-31G, d, p). The distances in figure S33 and figures 33-26 were measured by Vesta.

Single Crystal X-ray Diffraction experimental

Diffraction data were collected on a range of modern instruments equipped with area detectors, sealed-tube or rotating anode X-ray sources, and collected at low temperature. The data were corrected for absorption and Lp effects. Structures were solved by direct or a dual-space charge-flipping algorithm.[3,4] The structures were refined by full-matrix least-sqaures methods.[5] In common with other MOF crystals, this set of eleven copounds exhibited a range of behavious from very well behaved to problematic. The problems ranged from twinning issues which were sometimes resolved, or partially so, to others where a twin law could not be determined. Solvent of crystallisation could sometimes be easily modelled as point atoms, but in many cases was too disordered for this to be possible. In those cases the Platon Squeeze procedure was employed and the details have been given in the main manuscript for each structure.[6,7] In each case the chemical formulae include the 'Squeezed' solvent of crystallisation. The structures with highest *R*-factors give the general connectivity, but the fine details of geometry are less reliable in these cases. There can be some confidence in the connectivity for the less well determined structures **4**·2DMF and **7**·6DMF in particular, since they are isomorphic with the closely related **5**·2DMA and **8**·2.5DMF which are much better deterimed. H atoms were constrained except on hetero atoms (N, O) when the data were of sufficient quality to reveal their positions, in which case coordinates were refined, with mild geometrical restraints, if required. Where disorder was modelled both geometry and anisotropic displacement parameters were supported with the use of restraints.

CCDC 2207267-2207277 contain the supplementary crystallographic data for this paper. These data can be obtained free of charge from The Cambridge Crystallographic Data Centre via www.ccdc.cam.ac.uk/structures.

ROP of ε-Caprolactone and δ-valerolactone

All reactions need under nitrogen atmosphere were carried out in Schlenk tubes. ε-CL or δ-VL was polymerized using catalysts **1-11** as a melt. Complexes were weighed out by electric balance and then monomer was added to the flask by syringe. The reaction mixture was then placed into an oil bath preheated to the required temperature. The reaction was quenched by the addition of glacial acetic acid (0.2 mL), then was poured into cold methanol (10 mL). The reaction conversion was monitored by ^{1}H NMR (400 MHz, $CDCl_3$, 25 °C) spectroscopic studies. The resulting polymer was collected after vapour and dried in fume cupboard. GPC (in THF) were used to determine molecular weights (M_n and PDI) of the polymer products.

Polymerization Kinetics

Kinetic experiments were carried out following the previous polymerization method. At regular time intervals, 0.05 mL aliquots were removed, quenched with wet $CDCl_3$ (1 mL), and analyzed by ^1H NMR spectroscopy.

Synthesis of $\{[Zn(5\text{-AIP})(4,4^{/}\text{-bipy})_{0.5}]\cdot DMF\}_n$ (**1**·DMF)

5-Aminoisophthalic acid (0.50 mmol, 0.09 g), $Zn(NO_3)_2\cdot 6H_2O$ (0.75 mmol, 0.22 g) and 4,4/-bipyridine (0.38 mmol, 0.06 g) were dissolved in a DMF/methanol mixture (12 ml, 1:1) in 23 ml Teflon lined steel reaction vessel. The vessel was sealed and heated to 80 °C for 48 h, and then cooled at rate of 2 °C/h to room temperature, yielding 0.194 g of colourless hexagonal prisms of **1** (yield 80 % based on Zn). Elem. anal. calcd. for $C_{26}H_{18}N_4O_8Zn_2\cdot 2H_2O$: C 45.84, H 3.26, N 8.22%; found: C 45.81, H 2.96, N 8.50%; IR (KBr, cm^{-1}) 3430(w), 3249(m), 3134(w), 1668(s), 1614(s), 1574(s), 1538(w), 1494(w), 1441(m), 1420(w), 1345(s), 1248(m), 1226(w), 1189(w), 1133(m), 1100(s), 1048(w), 1016(w), 962(s), 933(m), 893(w), 826(m), 794(s), 778(s), 731(s) 679(m), 658(w), 644(m).

Synthesis of $\{[Zn(5\text{-AIP})(4,4^{/}\text{-azopy})_{0.5}]\cdot 0.75DMF\}_n$ (**2**·0.75DMF)

5-Aminoisophthalic acid (0.50 mmol, 0.09 g), $Zn(NO_3)_2\cdot 6H_2O$ (0.75 mmol, 0.22 g) and 4,4/-azopyridine (0.38 mmol, 0.07 g) were dissolved in a DMF/methanol mixture (12ml, 1:1) in 23ml Teflon lined steel reaction vessel. The vessel was sealed and heated to 80 °C for 48 h, and then cooled at rate of 2 °C/h to room temperature. The reaction yielded 0.15 g of orange prisms of **2** (yield 60 % based on Zn). Elem. anal. calcd. for $C_{26}H_{18}N_6O_8Zn_2$: C 46.38, H 2.69, N 12.48%; found: C 46.20, H 2.79, N 12.42%; IR (KBr, cm^{-1}) 3445(w), 3337(w), 2361(w), 1692(w), 1674(s), 1609(m), 1569(m), 1544(m), 1499(w), 1324(w), 1253(w), 1220(w), 1206(w), 1091(m), 1017(w), 1004(w), 980(w), 935(w), 892(w), 836(m), 807(w), 775(m), 726(m), 659(m), 554(m).

Synthesis of $\{[Co_2(NO_3)_2(5\text{-AIP})(4,4^{/}\text{-bipy})_2]\cdot 2EtOH\}_n$ (**3**·2EtOH)

5-Aminoisophthalic acid (0.50 mmol, 0.09 g), $Co(NO_3)_2\cdot 6H_2O$ (0.52 mmol, 0.15 g) and 4,4/-bipyridine (0.51 mmol, 0.08 g) were dissolved in a DMF/ethanol mixture (12 ml, 1:1) in 23 ml Teflon lined steel reaction vessel. The vessel was sealed and heated to 80 °C for 48 h, and then cooled at rate of 2 °C/h to room temperature. The reaction yielded 0.29 g of purple hexagonal

prisms of **3** (yield 80 % based on Co). Elem. anal. calcd. for $C_{28}H_{21}Co_2N_7O_{10}\cdot 4C_2H_6O$: C 46.02, H 4.87, N 10.73%; found C 45.67, H 4.48, N 10.35%; IR (KBr, cm^{-1}) 3446(w), 3341(w), 3228(w), 1677(s), 1603(m), 1571(m), 1547(m), 1411(w), 1325(w), 1220(w), 1094(w), 1005(w), 1046(w), 1005(w), 968(w), 937(w), 892(w), 816(m), 775(m), 727(m), 660(w), 633(w).

Synthesis of $\{[Co(5\text{-}AIP)(DPE)]\cdot 2DMF\}_n$ (**4**·2DMF)

5-Aminoisophthalic acid (0.50 mmol, 0.09 g), $Co(NO_3)_2\cdot 6H_2O$ (0.52 mmol, 0.15 g) and DPE (0.5 mmol, 0.09 g) were dissolved in DMF/ethanol (12 ml, 1:1) in 23 ml Teflon lined steel reaction vessel. The vessel was sealed and heated to 80 °C for 48 h, and then cooled at rate of 2 °C/h to room temperature, yielding 0.17 g of purple prisms of **4** (80 % based on Co). Elem. anal. calcd. for $C_{20}H_{15}CoN_3O_4$: C 57.16, H 3.60, N 10.00%; found C 57.25, H 3.77, N 9.87%; IR (KBr, cm^{-1}) 3436(w), 3248(w), 3133(w), 1675(s), 1616(s), 1573(s), 1506(w), 1441(m), 1340(s), 1248(m), 1226(w), 1211(w), 1132(m), 1096(s), 1028(m), 1002(w), 987(w), 961(m), 932(w), 893(w), 843(m), 794(m), 778(m), 730(s), 678(m), 659(m).

Synthesis of $\{[Co(5\text{-}AIP)(4,4'\text{-azopy})]\cdot 2DMA\}_n$ (**5**·2DMA)

5-Aminoisophthalic acid (0.5 mmol, 0.09 g), $Co(NO_3)_2\cdot 6H_2O$ (0.52 mmol, 0.15 g) and 4,4′-azopyridine (0.5 mmol, 0.09 g) were dissolved in DMA/ethanol (12 ml, 1:1) in 23 ml Teflon lined steel reaction vessel. The vessel was sealed and heated to 80 °C for 48 h, and then cooled at rate of 2 °C/h to room temperature to afford 0.12 g of dark red prisms of **5** (58 % based on Co). Elem. anal. calcd. for $C_{18}H_{13}CoN_5O_4$: C 51.20, H 3.10, N 16.59%; found C 51.10, N 3.10, N 16.45%; IR (KBr, cm^{-1}) 3451(w), 3343(w), 3231(w), 1677(s), 1601(w), 1570(m), 1544(w), 1416(w), 1326(w), 1256(w), 1225(w), 1091(m), 1055(w), 1017(w), 964(w), 892(w), 848(w), 776(m), 726(m), 680(w), 660(w).

Synthesis of $\{[Mn(5\text{-}AIP)(4,4'\text{-bipy})]\cdot 2DMA\}_n$ (**6**·2DMA)

$Mn(NO_3)_2\cdot 4H_2O$ (0.52 mmol, 0.13 g), 5-aminoisophthalic acid (0.50 mmol, 0.09 g) and 4,4′-bipyridine (0.51 mmol, 0.08 g) were dissolved in DMA/methanol (12 ml, 1:1) and sealed in a 23 ml Teflon lined steel reaction vessel. The vessel was sealed and heated to 80 °C for 48 h, and then cooled at a rate of 2 °C/h to room temperature, yielding 0.12 g of yellow prisms of **6** (61 % based on Mn). Elem. anal. calcd. for $C_{18}H_{13}MnN_3O_4$: C 55.40, H 3.36, N 10.77%; found C 55.26, H 3.45, N 10.89%; IR (KBr, cm^{-1}) 3452(w), 3344(m), 3225(w), 1673(s), 1602(m), 1550(s), 1414(m),

1326(w), 1254(w), 1221(m), 1092(m), 1042(w), 1005(w), 933(w), 894(w), 813(s), 779(s), 728(s), 657(w), 629(m).

Synthesis of {[Mn(5-AIP)(DPE)]·6DMF}$_n$ (**7**·6DMF)

$Mn(NO_3)_2 \cdot 4H_2O$ (0.52 mmol, 0.13 g), 5-aminoisophthalic acid (0.50 mmol, 0.09 g) and 1,2-bis(4-pyridyl)ethylene (0.49 mmol, 0.09 g) were dissolved in DMF/methanol (12 ml, 1:1) and sealed in a 23 ml Teflon lined steel reaction vessel. The vessel was sealed and heated to 80 °C for 48 h, and then cooled at a rate of 2 °C/h to room temperature. The reaction yielded 0.17 g of yellow prisms of **7** (82 % based on Mn). Elem. anal. calcd. for $C_{20}H_{15}MnN_3O_4$: C 57.70, H 3.63, N 10.09%; found C 57.55, H 3.75, N 10.15%; IR (KBr, cm^{-1}) 3457(w), 3339(m), 3225(w), 1675(s), 1609(m), 1550(s), 1326(s), 1254(w), 1220(w), 1091(w), 1070(w), 1016(w), 969(w), 956(w), 894(w), 827(m), 807(w), 779(m), 728(s).

Synthesis of {[Mn(5-AIP)(Azopy)]·2.5DMF}$_n$ (**8**·2.5DMF)

$Mn(NO_3)_2 \cdot 4H_2O$ (0.52 mmol, 0.13 g), 5-aminoisophthalic acid (0.50 mmol, 0.09 g) and 4,4′-azopyridine (0.5 mmol, 0.09 g) were dissolved in DMF/methanol (12 ml, 1:1) and sealed in a 23 ml Teflon lined steel reaction vessel. The vessel was sealed and heated to 80 °C for 48 h, and then cooled at a rate of 2 °C/h to room temperature. The reaction yielded 0.12 g of red prisms of **8** (61 % based on Mn). Elem. anal. calcd. for $C_{18}H_{13}MnN_5O_4$: C 51.69, H 3.13, N 16.74%; found C 51.53, H 3.27, N 16.57%; IR (KBr, cm^{-1}) 3452(w), 3343(m), 3230(w), 1676(s), 1600(m), 1550(s), 1416(w), 1326(w), 1254(w), 1225(w), 1090(w), 1055(w), 1013(w), 1006(w), 933(w), 894(w), 864(m), 809(w), 779(m), 728(s).

Synthesis of {[Cd(5-AIP)(4,4′-bipy)]·3DMF}$_n$ (**9**·3DMF)

$Cd(NO_3)_2 \cdot 4H_2O$ (0.49 mmol, 0.15 g), 5-aminoisophthalic acid (0.50 mmol, 0.09 g) and 4,4′-bipyridine (0.51 mmol, 0.08 g) were dissolved in DMF/methanol (12 ml, 1:1) and sealed in a 23 ml Teflon lined steel reaction vessel. The vessel was heated to 80 °C for 48 h, and then cooled at a rate of 2 °C/h to room temperature, yielding 0.18 g of colourless prisms of **9** (82 % based on Cd). Elem. anal. calcd. for $C_{18}H_{13}CdN_3O_4 \cdot C_3H_7NO$: C 48.43, H 3.87, N 10.76%; found C 48.15, H 3.52, N 10.66 %; IR (KBr, cm^{-1}) 3350(w), 3221(w), 1669(s), 1653(w), 1603(s), 1545(s), 1517(w), 1413(w), 1320(w), 1253(w), 1220(w), 1166(w), 1150(w), 1094(m), 1068(m), 1044(m), 1008(w), 965(w), 934(w), 898(w), 856(w), 814(w), 778(s), 732(s), 657(w), 631(w).

Synthesis of {[Cd(5-AIP)(DPE)]·4.5DMF }$_n$ (**10**·4.5DMF)

$Cd(NO_3)_2·4H_2O$ (0.49 mmol, 0.15 g), 5-aminoisophthalic acid (0.50 mmol, 0.09 g) and 1,2-bis(4-pyridyl)ethylene (0.5 mmol, 0.09 g) were dissolved in DMF/methanol (12 ml, 1:1) and sealed in a 23 ml Teflon lined steel reaction vessel. The vessel was heated to 80 °C for 48 h, and then cooled at a rate of 2 °C/h to room temperature. The reaction yielded 0.14 g of pale yellow prisms of **10** (57 % based on Cd). Elem. anal. calcd. for $C_{20}H_{15}CdN_3O_4$: C 50.70, H 3.19, N 8.87%; found C 50.65, H 3.10, N 8.78%; IR (KBr, cm^{-1}) 3351(s), 3221(w), 1665(s), 1698(s), 1544(s), 1502(w), 1495(w), 1427(s), 1325(w), 1252(w), 1221(w), 1207(w), 1169(w), 1150(w), 1096(m), 1070(w), 1017(m), 1004(w), 1017(m), 1004(w), 977(w), 935(w), 898(w), 864(w), 832(m), 808.4(w), 779(s), 731(s), 660(w).

Synthesis of {[Cd(5-AIP)(4,4$^{/}$-azopy)(DMF)}$_n$ (**11**)

$Cd(NO_3)_2·4H_2O$ (0.49 mmol, 0.15 g), 5-aminoisophthalic acid (0.50 mmol, 0.09 g) and 4,4$^{/}$-azopyridine (0.49 mmol, 0.09 g) were dissolved in DMF/methanol (12 ml, 1:1) and sealed in a 23 ml Teflon lined steel reaction vessel. The vessel was heated to 80 °C for 48 h, and then cooled at a rate of 2 °C/h to room temperature. The reaction yielded 0.15 g of dark red prisms of **11** (54 % based on Cd). Elem. anal. calcd. for $C_{18}H_{13}CdN_5O_4·C_3H_7NO$: C 45.96, H 3.67, N 15.31%; found C 45.80, H 3.69, N 15.04%; IR (KBr, cm^{-1}) 3259(w), 3184(w), 1653(s), 1648(s), 1609(m), 1559(m), 1545(m), 1517(w), 1507(w), 1499(w), 1424(w), 1318(m), 1263(w), 1224(w), 1195(w), 1172(w), 1127(w), 1087(m), 1052(w), 1027(w), 1016(m), 998(w), 970(m), 941(w), 912(w), 887(w), 848(w), 836(w), 801(m), 777(m), 723(s), 665(w).

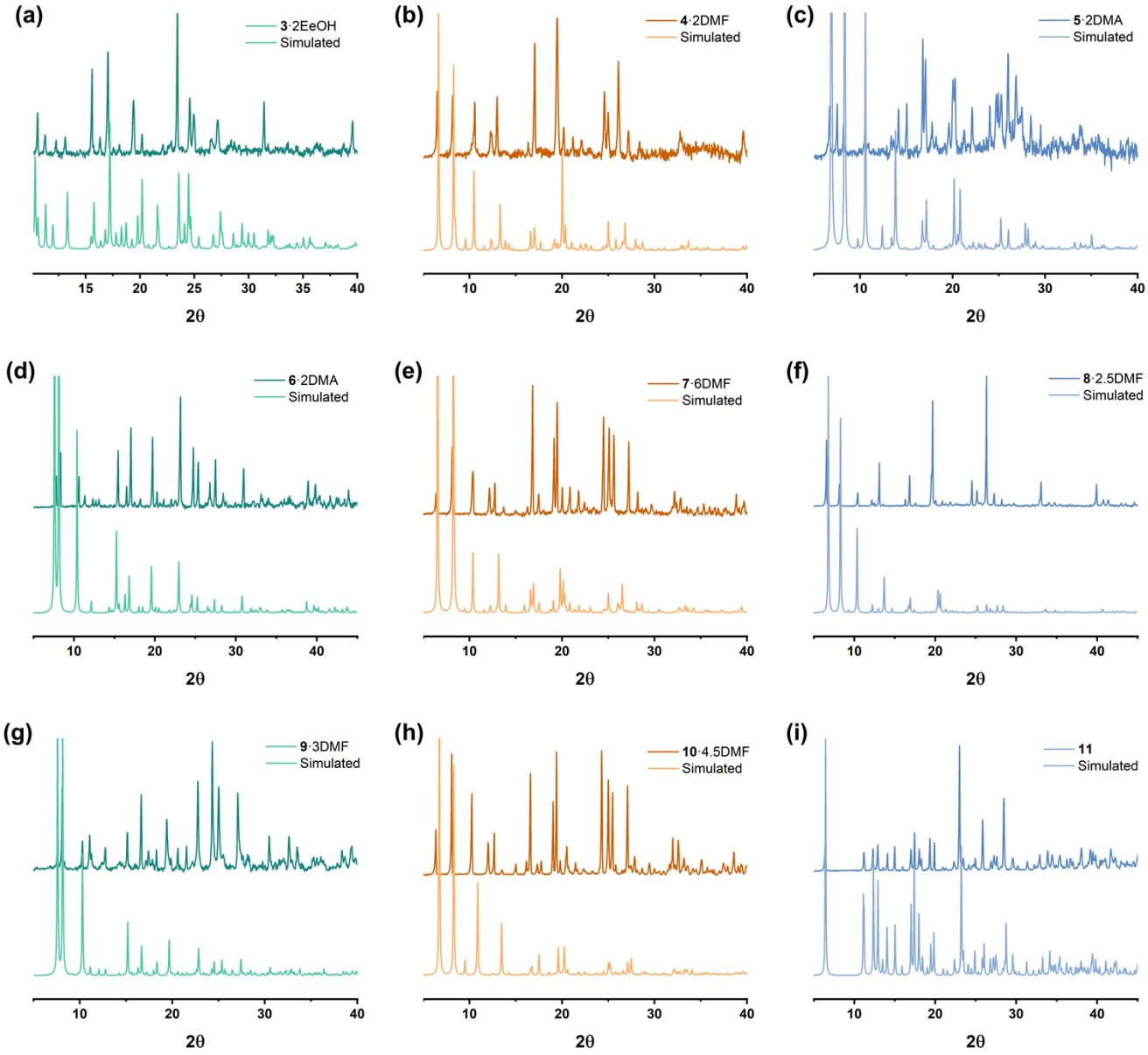

Figure S1. Powder x-ray diffraction of (a) **3**·2EtOH; (b) **4**·2DMF; (c) **5**·2DMA; (d) **6**·2DMA; (e) **7**·6DMF; (f) **8**·2.5DMF; (g) **9**·3DMF; (h) **10**·4.5DMF; (i) **11**.

TGA results

In order to further investigate their structural characteristics, thermogravimetric investigations of **1**–**11** presented here were carried out between 30 and 600 °C with an inert carrier flow (nitrogen). Weight loss of solvent molecules are marked in the **1**-**10** TGA curves (Figure S2). Calculated 18% weight loss between 153-412 °C was attributed to the loss of one DMF molecule per formula unit from **1**·DMF (Figure S2(a)). Then the following weight loss was due to decomposition. Calculated 14% weight loss between 153-218 °C was attributed to the loss of 0.75 DMF molecule per formula unit from **2**·0.75DMF (Figure S2(b)). Then the following weight loss was due to decomposition. Calculated 11% weight loss between 78-100 °C was attributed to the loss of two EtOH molecule

per formula unit from **3**·2EtOH (Figure S2(c)). Then the following weight loss was due to decomposition. Calculated 26% weight loss between 153-341 °C was attributed to the loss of two DMF molecule per formula unit from **4**·2DMF (Figure S2(d)). Then the following weight loss was due to decomposition. Calculated 29% weight loss between 164-343 °C was attributed to the loss of two DMA molecule per formula unit from **5**·2DMA (Figure S2(e)). Then the following weight loss was due to decomposition. Calculated 41% weight loss between 164-345 °C was attributed to the loss of two DMA molecule per formula unit from **6**·2DMA and decomposition (Figure S2(f)). Then the following weight loss was due to decomposition. Calculated 43% weight loss between 153-362 °C was attributed to the loss of five DMF molecule per formula unit from **7**·6DMF (Figure S2(g)). Then the following weight loss was due to decomposition. Calculated 43% weight loss between 153-354 °C was attributed to the loss of 2.5 DMF molecule per formula unit from **8**·2.5DMF and decomposition (Figure S2(h)). Then the following weight loss was due to decomposition. Calculated 32% weight loss between 153-370 °C was attributed to the loss of three DMF molecule per formula unit from **9**·3DMF (Figure S2(i)). Then the following weight loss was due to decomposition. Calculated 43% weight loss between 153-380 °C was attributed to the loss of 4.5 DMF molecule per formula unit from **10**·4.5DMF (Figure S2(j)). Then the following weight loss was due to decomposition.

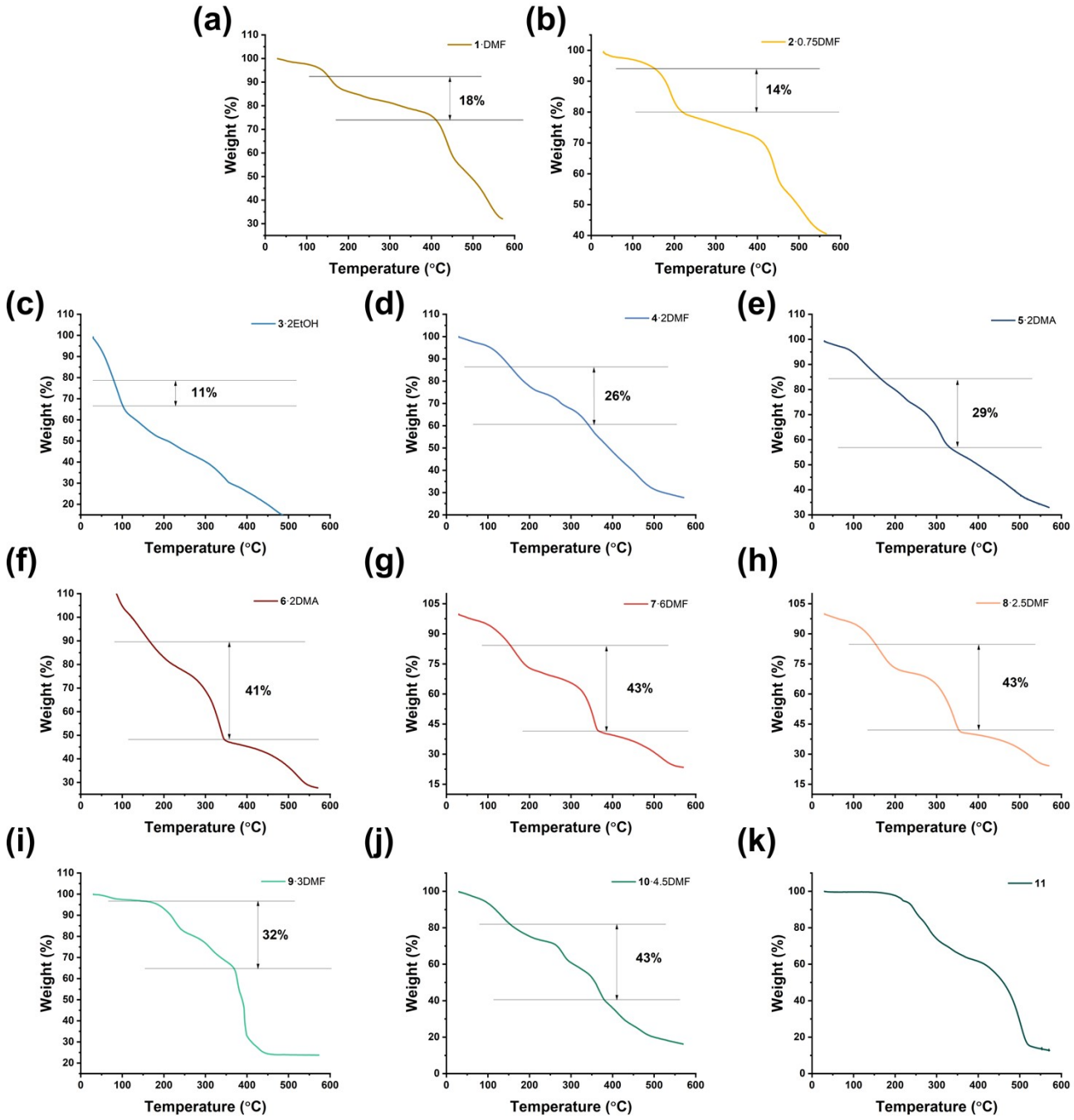

Figure S2. Thermogravimetric analyses of (a) **1**·DMF; (b) **2**·0.75DMF; (c) **3**·2EtOH; (d) **4**·2DMF; (e) **5**·2DMA; (f) **6**·2DMA; (g) **7**·6DMF; (h) **8**·2.5DMF; (i) **9**·3DMF; (j) **10**·4.5DMF; (k) **11**.

EDS results

EDS curves were used to examine the weight and atomic ratios of all elements in **1**·DMF (Figure **26** (a)). It is important to note that the result only reflects the distribution of elements on the surface. According to the formula of **1**·DMF ($C_{13}H_9N_2O_4Zn{\cdot}C_3H_7NO$), there is not enough zinc on the surface, indicating that there is more zinc in the interior. In addition, silicon and sulfur are impurities introduced during testing and can be ignored.

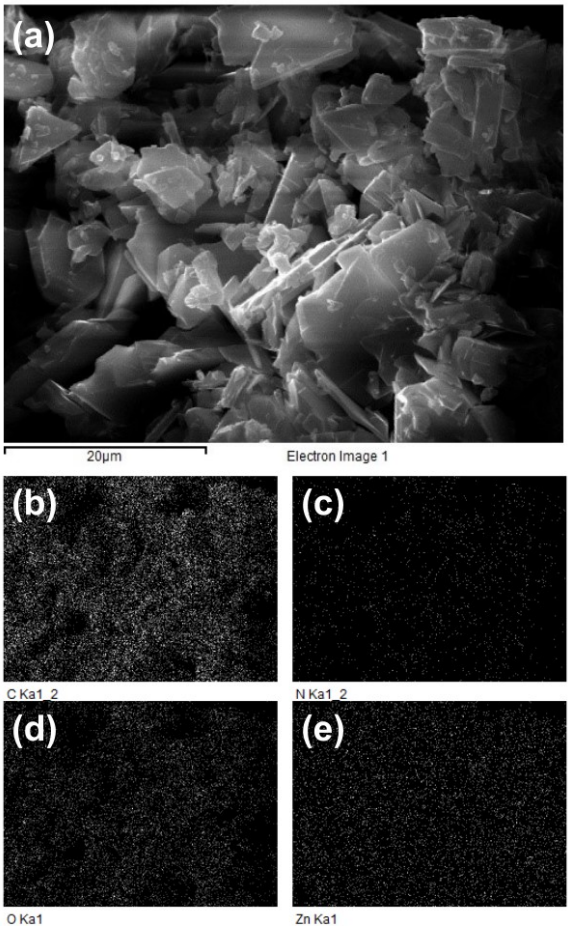

Figure S3. Mapping scanning of (a) **1**·DMF and its (b) Carbon, (c) Nitrogen, (d) Oxygen, (e) Zinc element scanning.

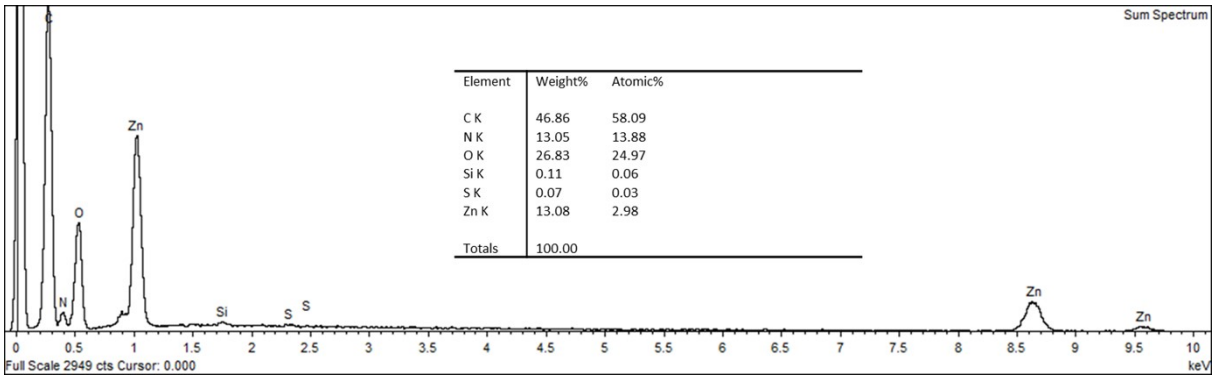

Figure S4. EDS curves of **1**·DMF.

BET results

Specific surface area and pore size were applied in BET tests. MOFs were activated to eliminate all guest molecules and degassed to remove all moisture prior to testing. The pore size of MOFs have a similar pore size distribution (Figure S5) but different surface area. According to the results of pore size, these MOFs are mesoporous material because most of them has size above 30 nm. For the zinc

complexes, the surface area of **2** (23.2926 m^2/g) is larger than **1** (13.0559 m^2/g). For the cobalt complexes, all of them show similar surface area (22.6328 m^2/g of **3**, 20.6058 m^2/g of **4**, 21.0169 m^2/g of **5**). Except for **6** (76.4750 m^2/g), which has the largest surface area, **7** (21.4121 m^2/g) has a typical result and **8** has a smaller one (4.5277 m^2/g). The surface areas of **9** (13.6891 m^2/g) and **10** (13.6604 m^2/g) are extremely closed, whereas the surface area of **11** (3.2624 m^2/g) is the lowest of all the complexes.

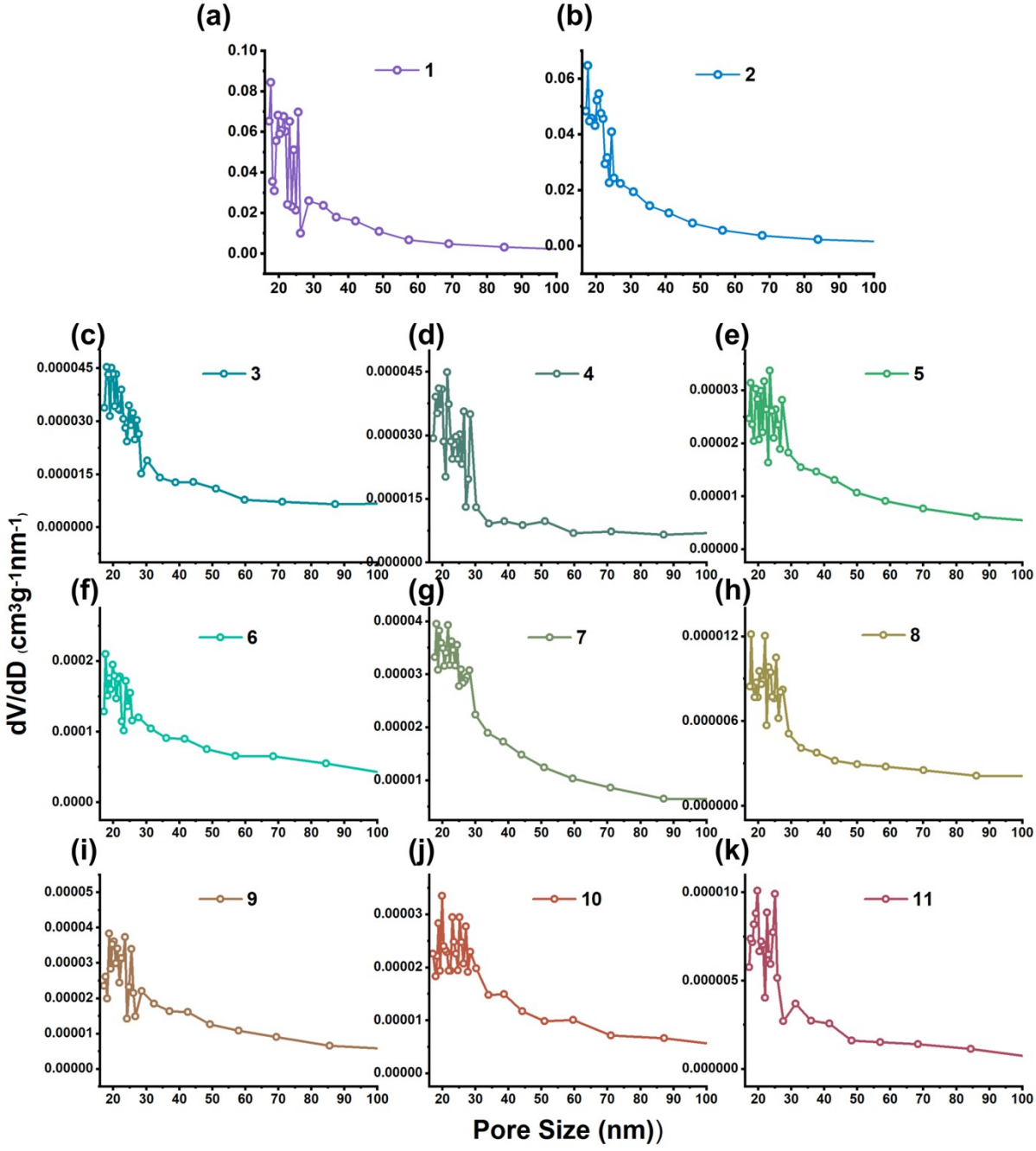

Figure S5. Pore size distribution of (a) **1**, (b) **2**, (c) **3**, (d) **4**, (e) **5**, (f) **6**, (g) **7**, (h) **8**, (i) **9**, (j) **10** and (k) **11**.

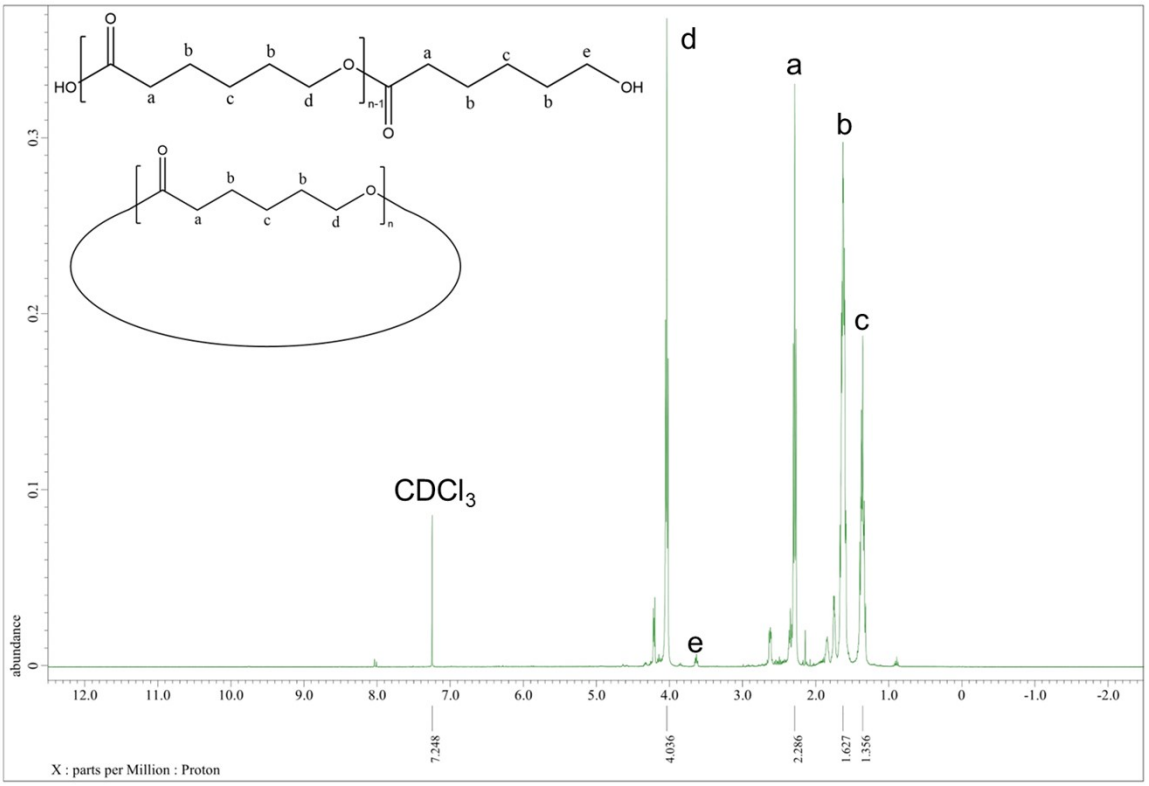

Figure S6. ^{1}H NMR spectrum for PCL (Table 1, entry 8).

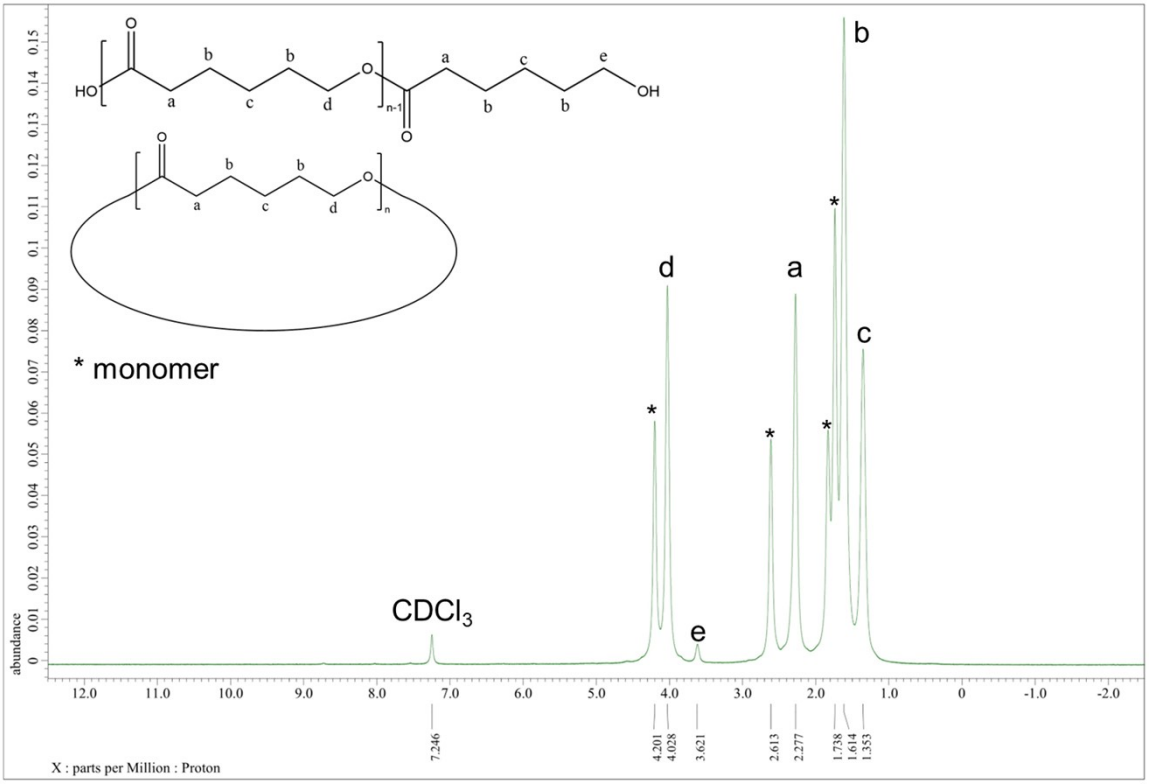

Figure S7. ^{1}H NMR spectrum for PCL (Table 1, entry 9).

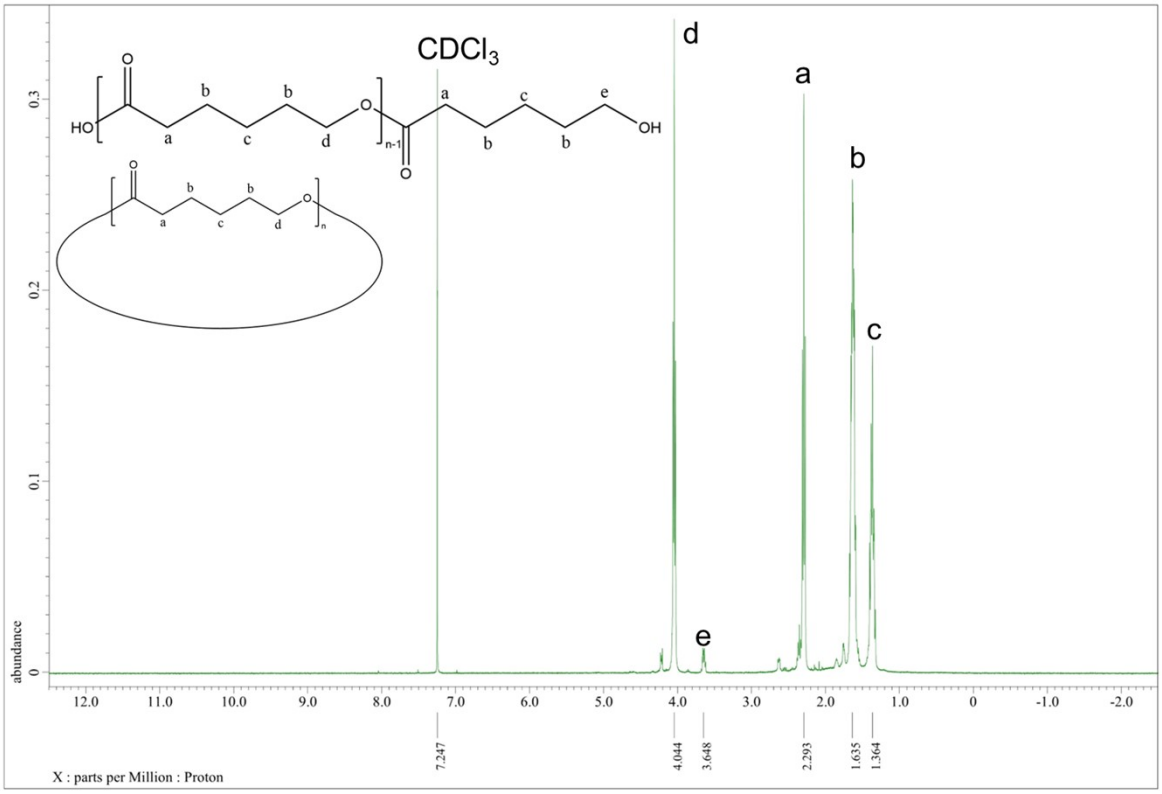

Figure S8. ^{1}H NMR spectrum for PCL (Table 1, entry 10).

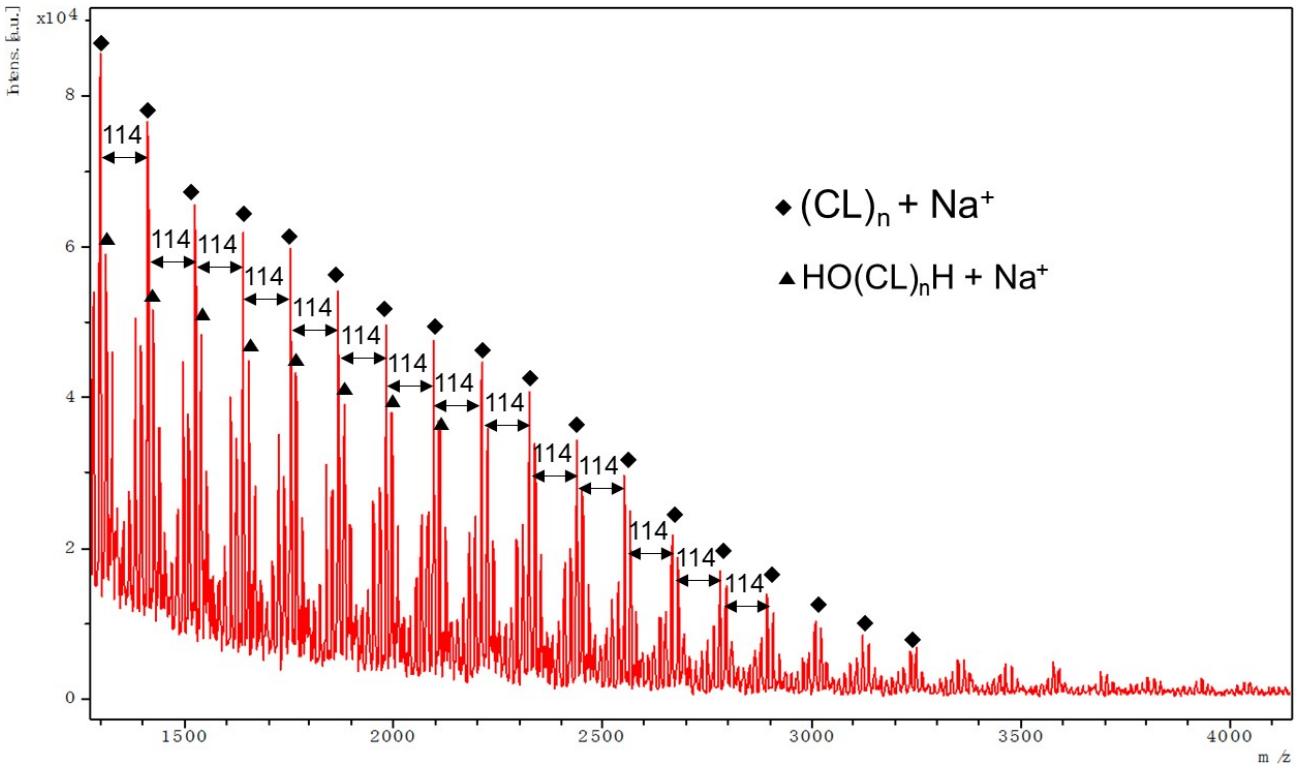

Figure S9. MALDI-TOF mass spectrum of PCL (Table 1, entry 8).

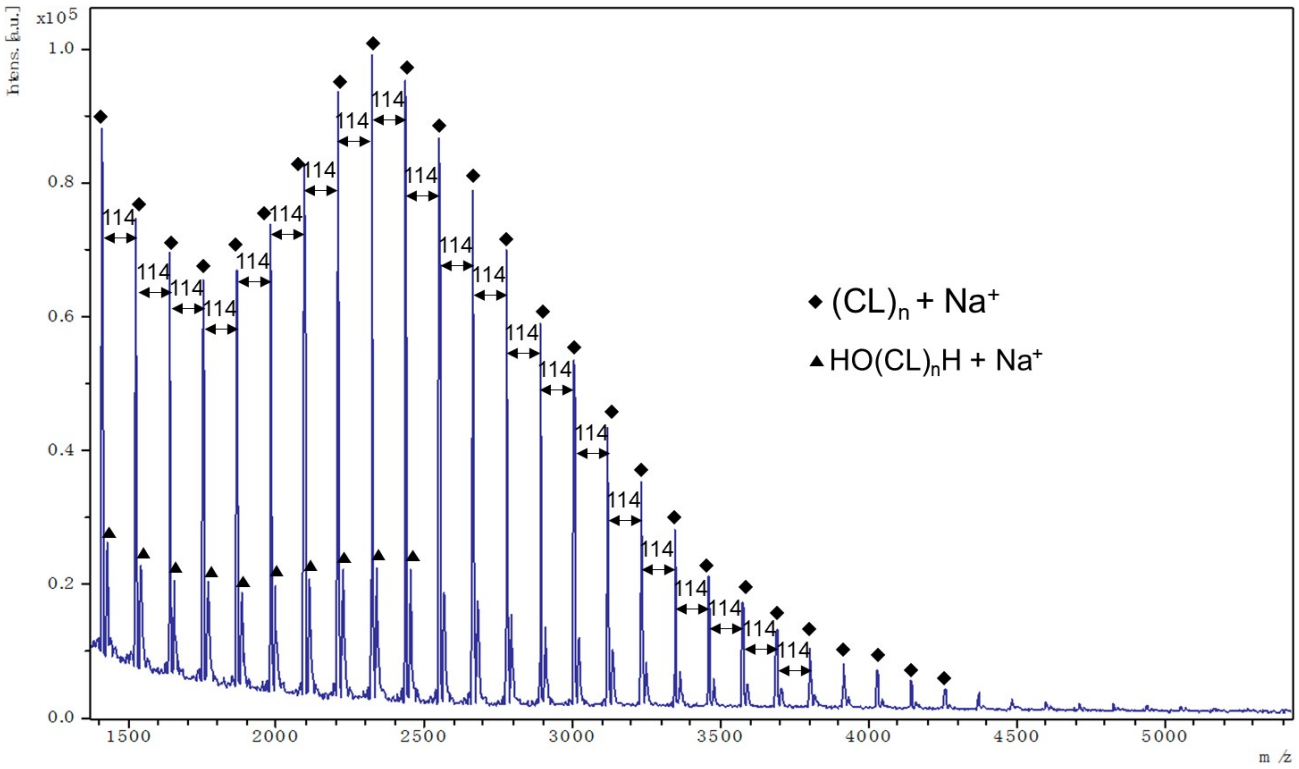

Figure S10. MALDI-TOF mass spectrum of PCL (Table 1, entry 9).

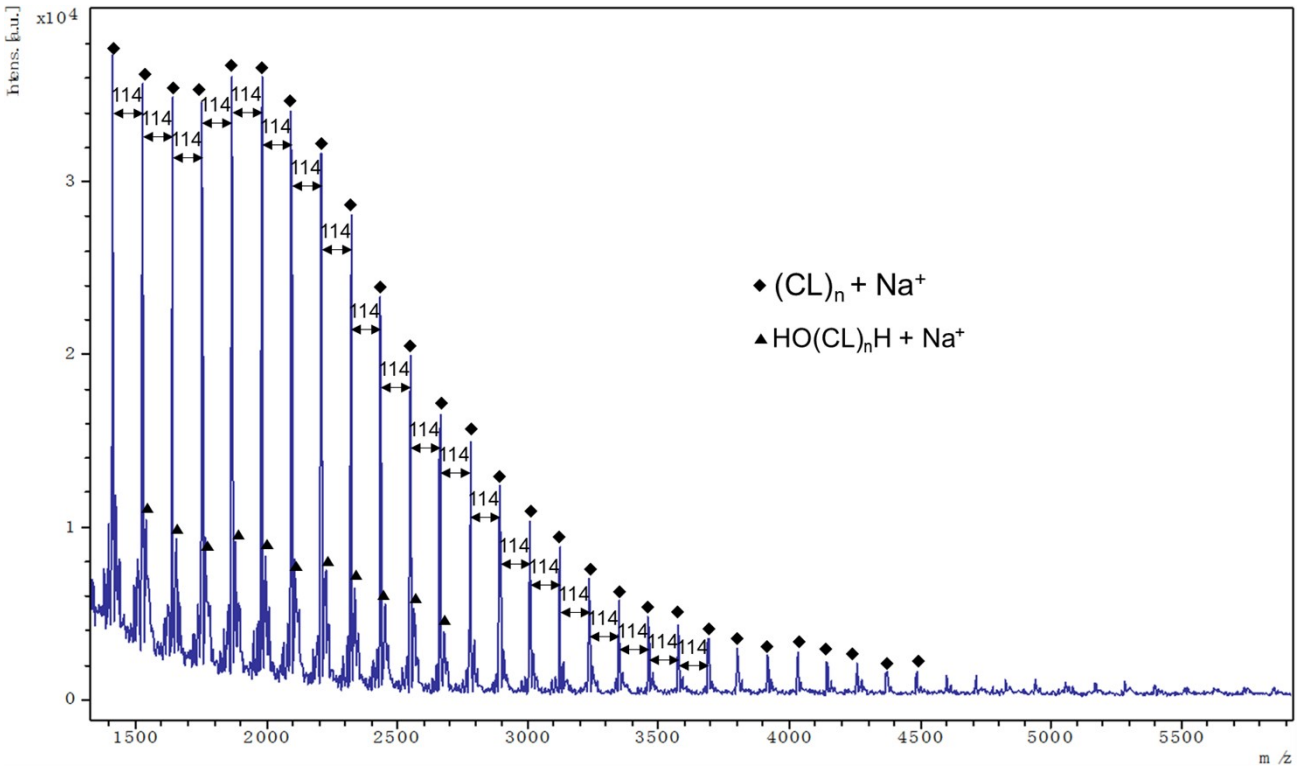

Figure S11. MALDI-TOF mass spectrum of PCL (Table 1, entry 10).

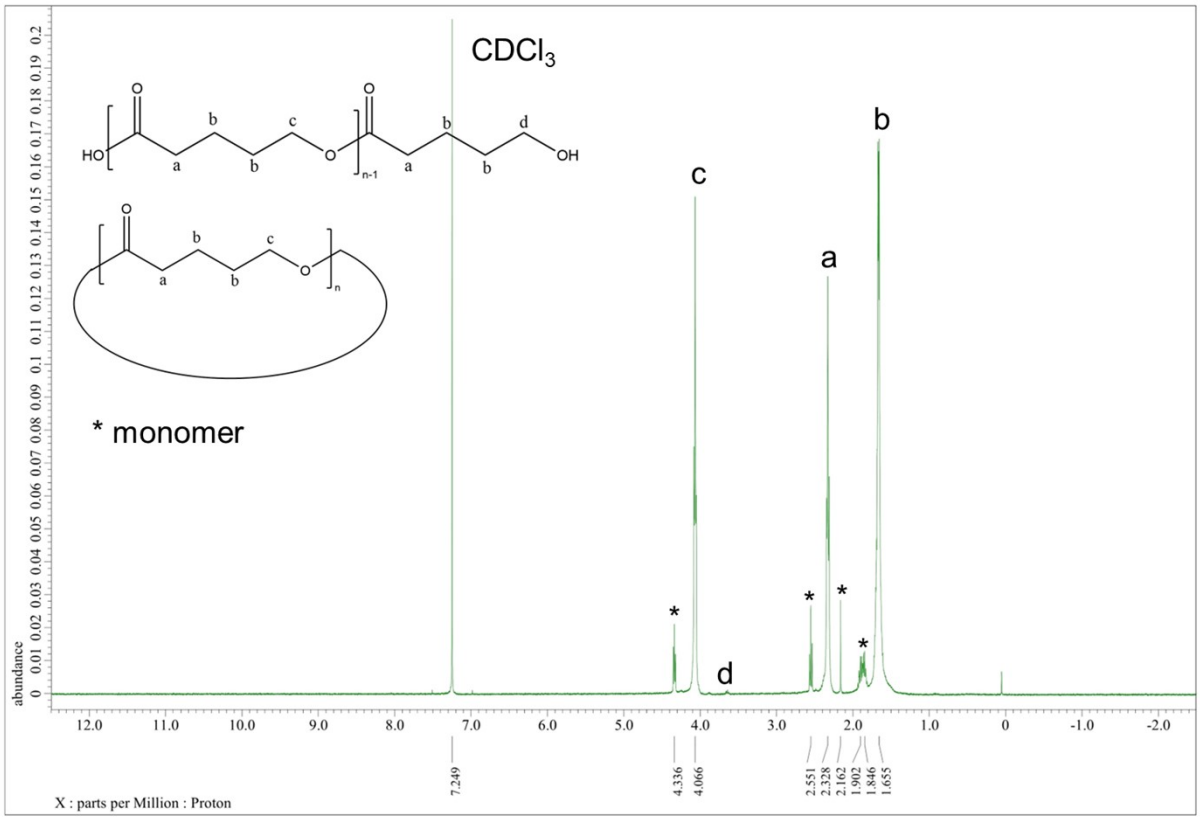

Figure S12. [1]H NMR spectrum for PVL (Table 2, entry 2).

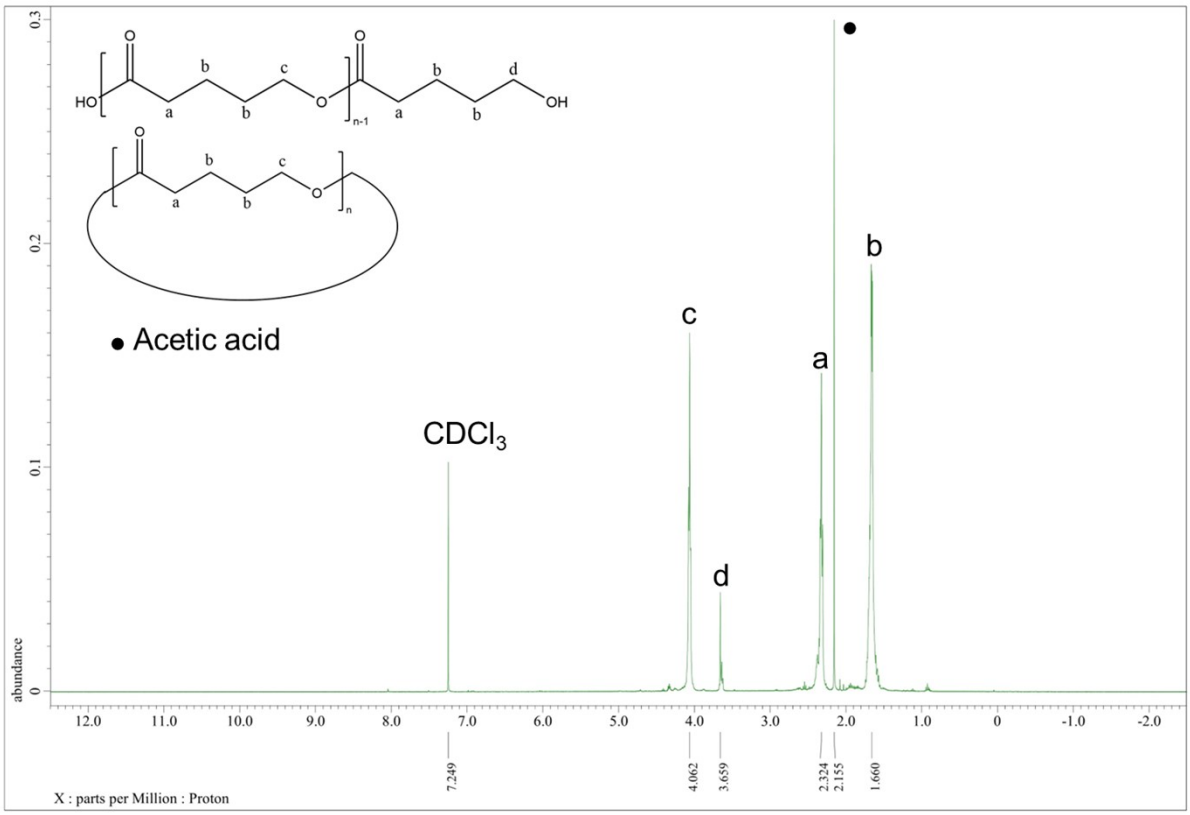

Figure S13. [1]H NMR spectrum for PVL (Table 2, entry 3).

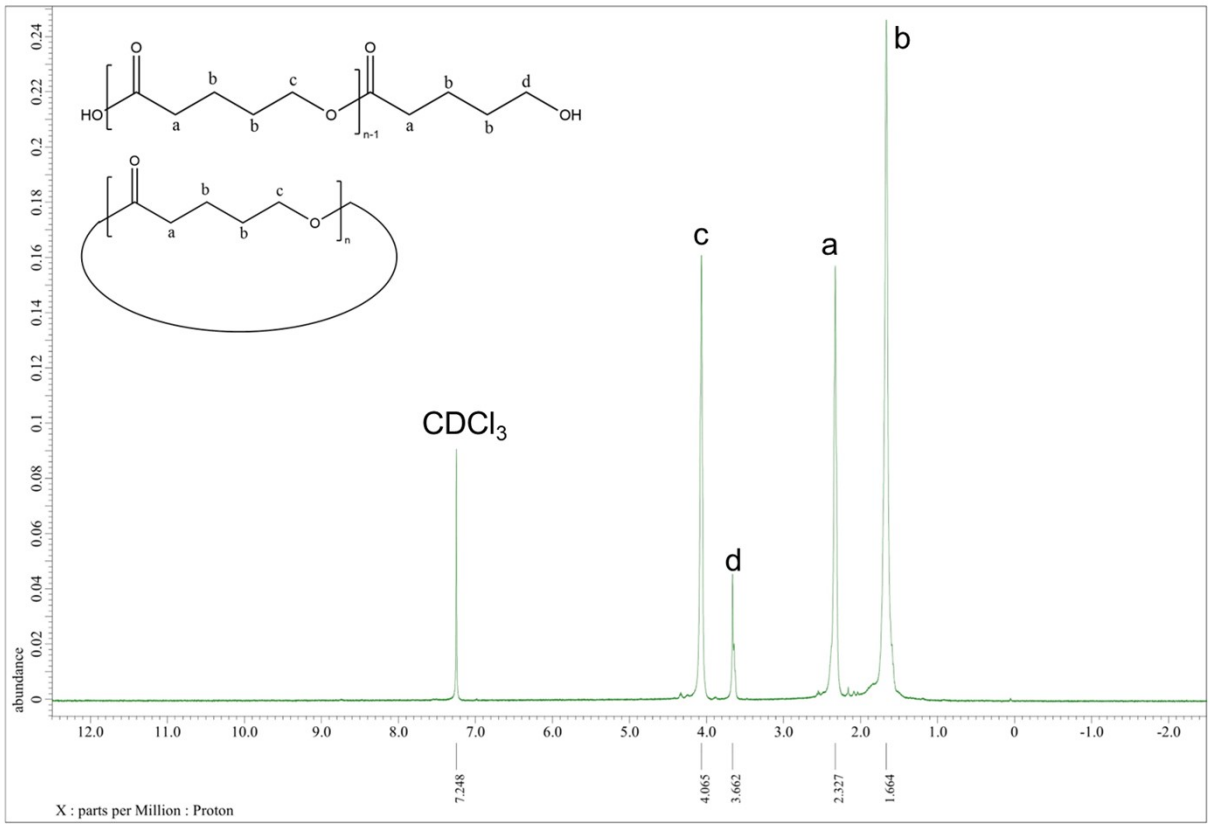

Figure S14. [1]H NMR spectrum for PVL (Table 2, entry 4).

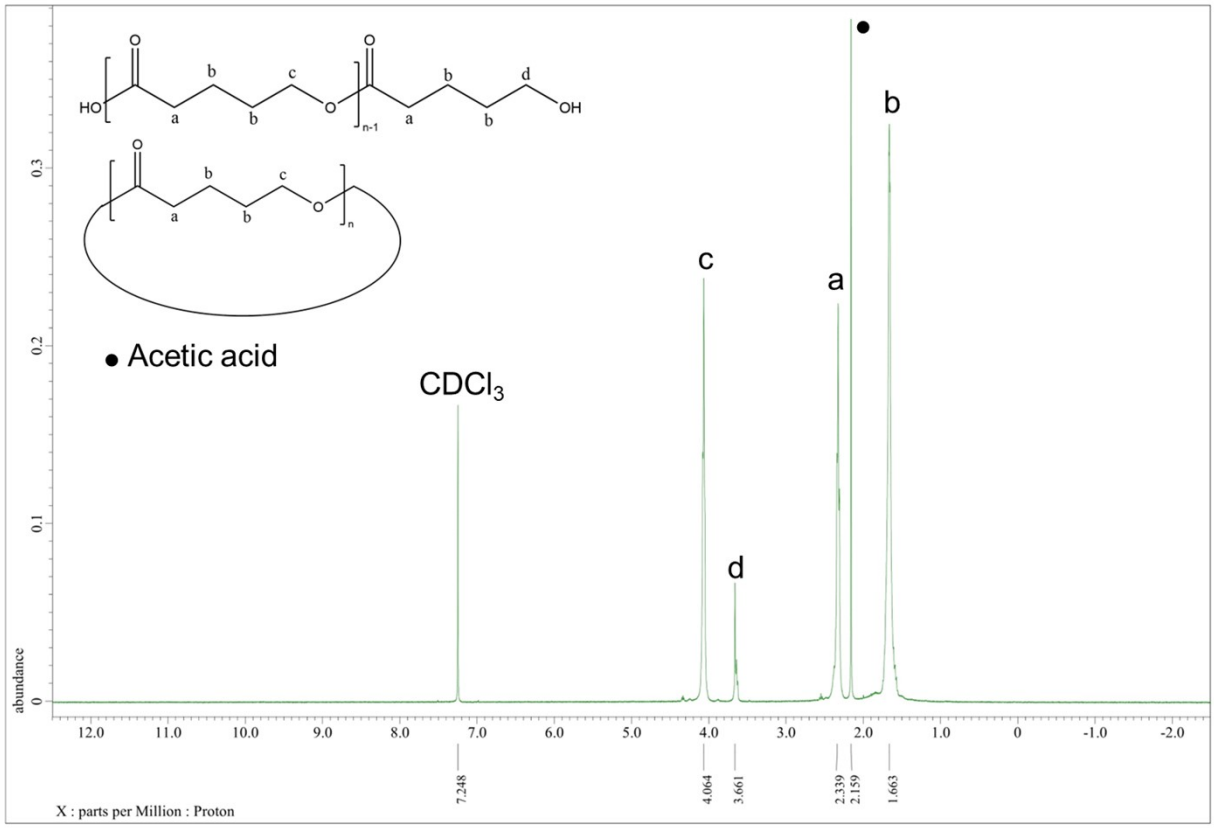

Figure S15. [1]H NMR spectrum for PVL (Table 2, entry 5).

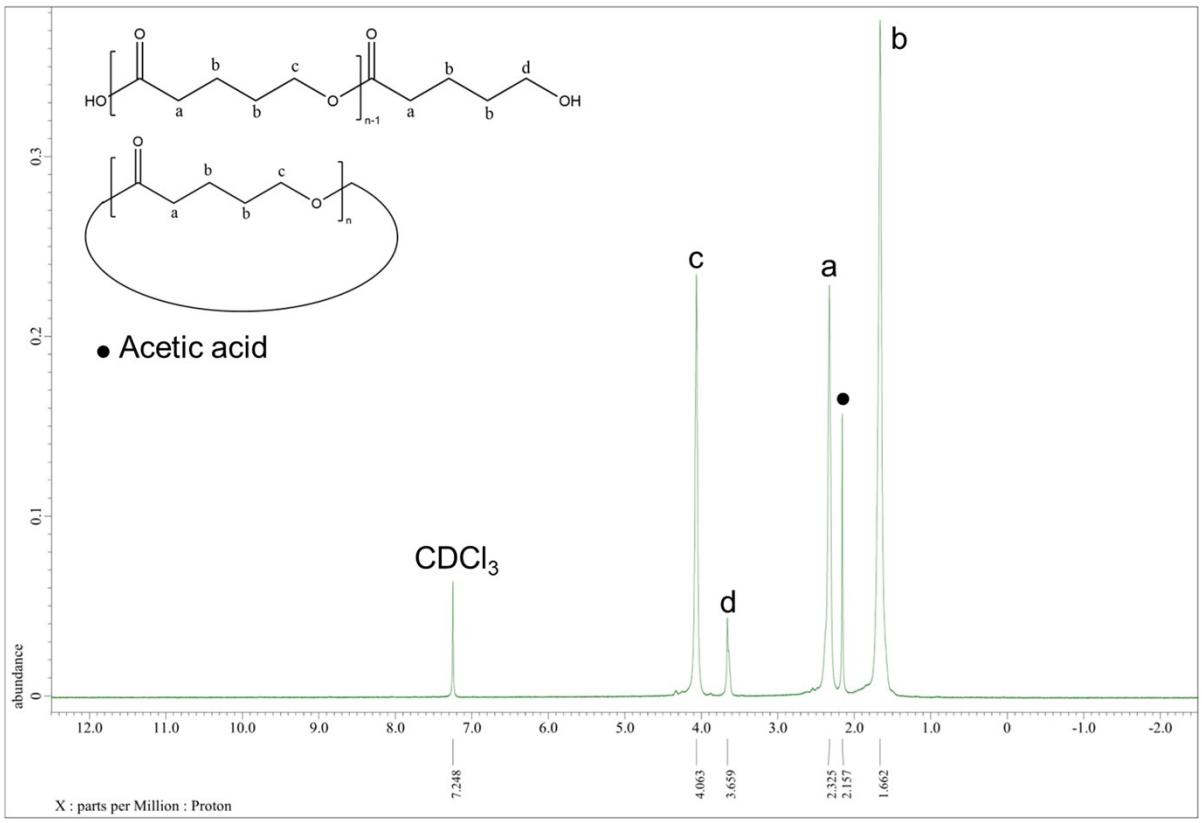

Figure S16. [1]H NMR spectrum for PVL (Table 2, entry 6).

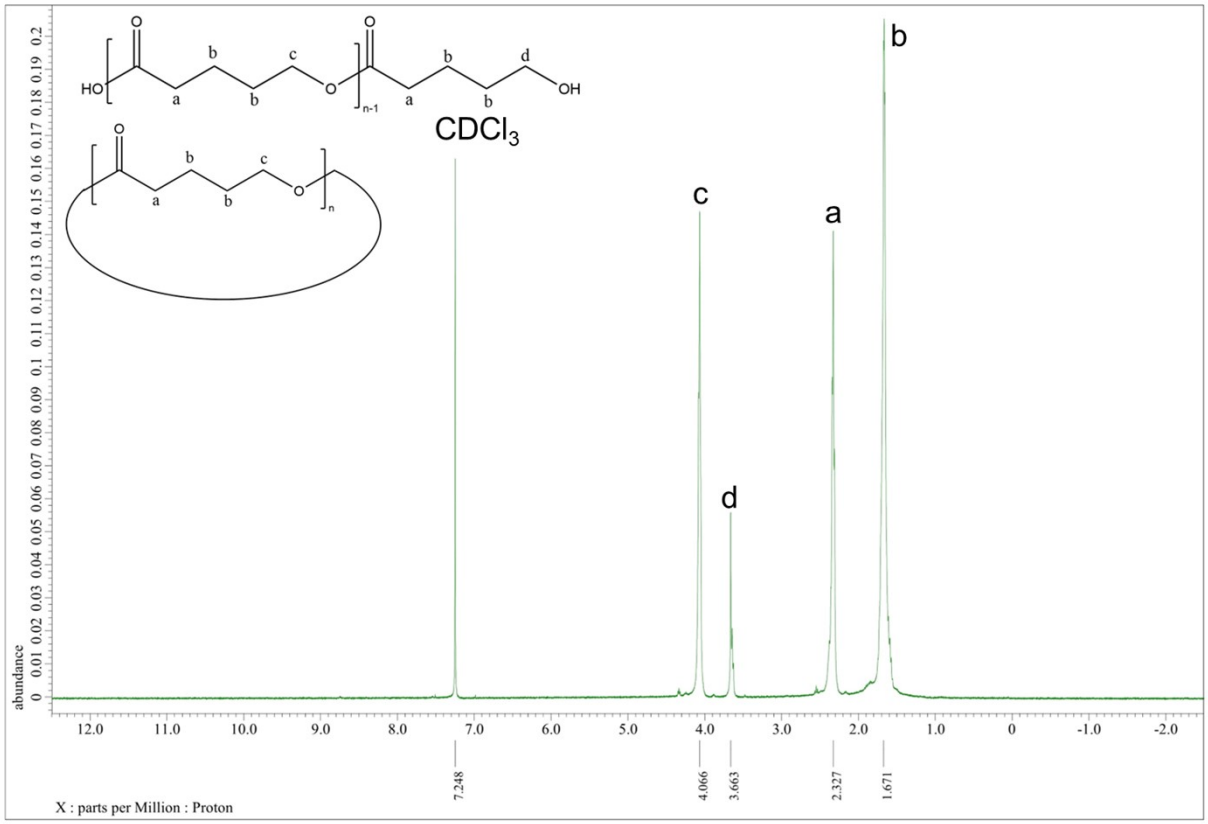

Figure S17. [1]H NMR spectrum for PVL (Table 2, entry 7).

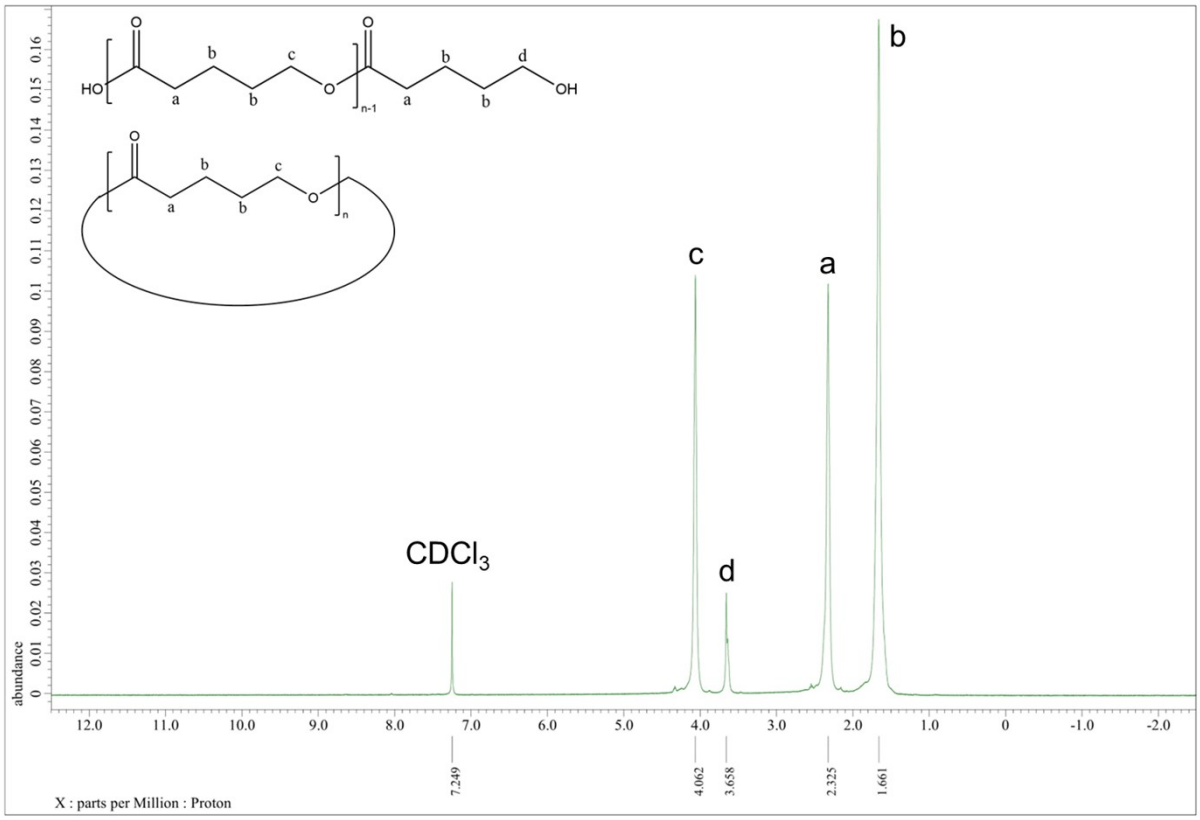

Figure S18. [1]H NMR spectrum for PVL (Table 2, entry 8).

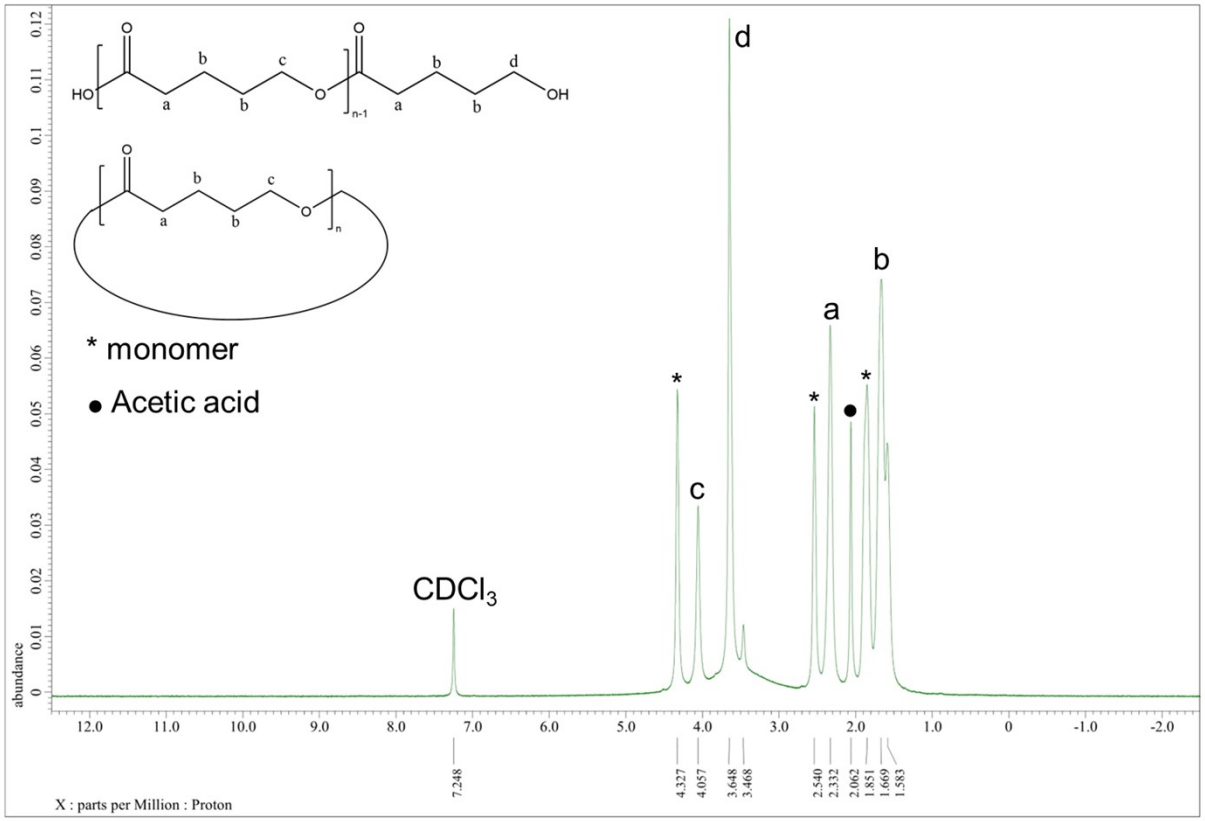

Figure S19. [1]H NMR spectrum for PVL (Table 2, entry 9).

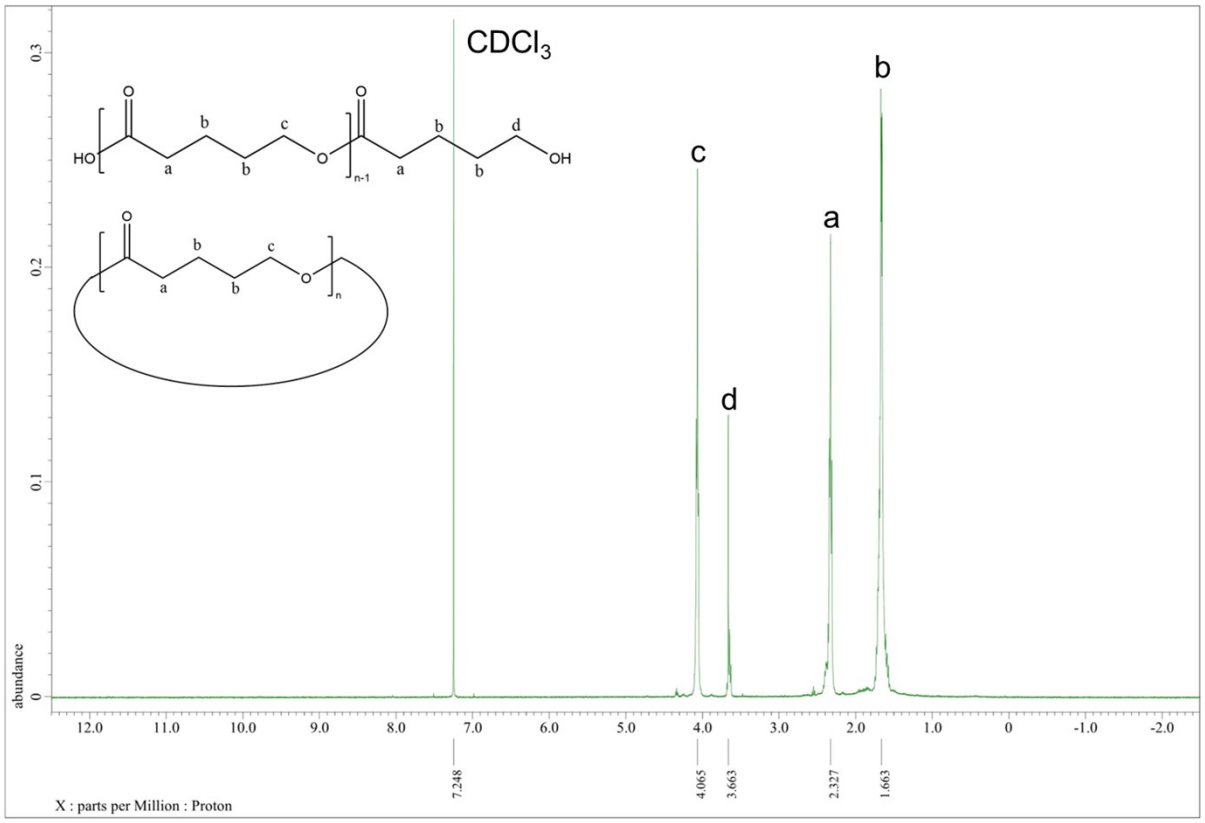

Figure S20. [1]H NMR spectrum for PVL (Table 2, entry 10).

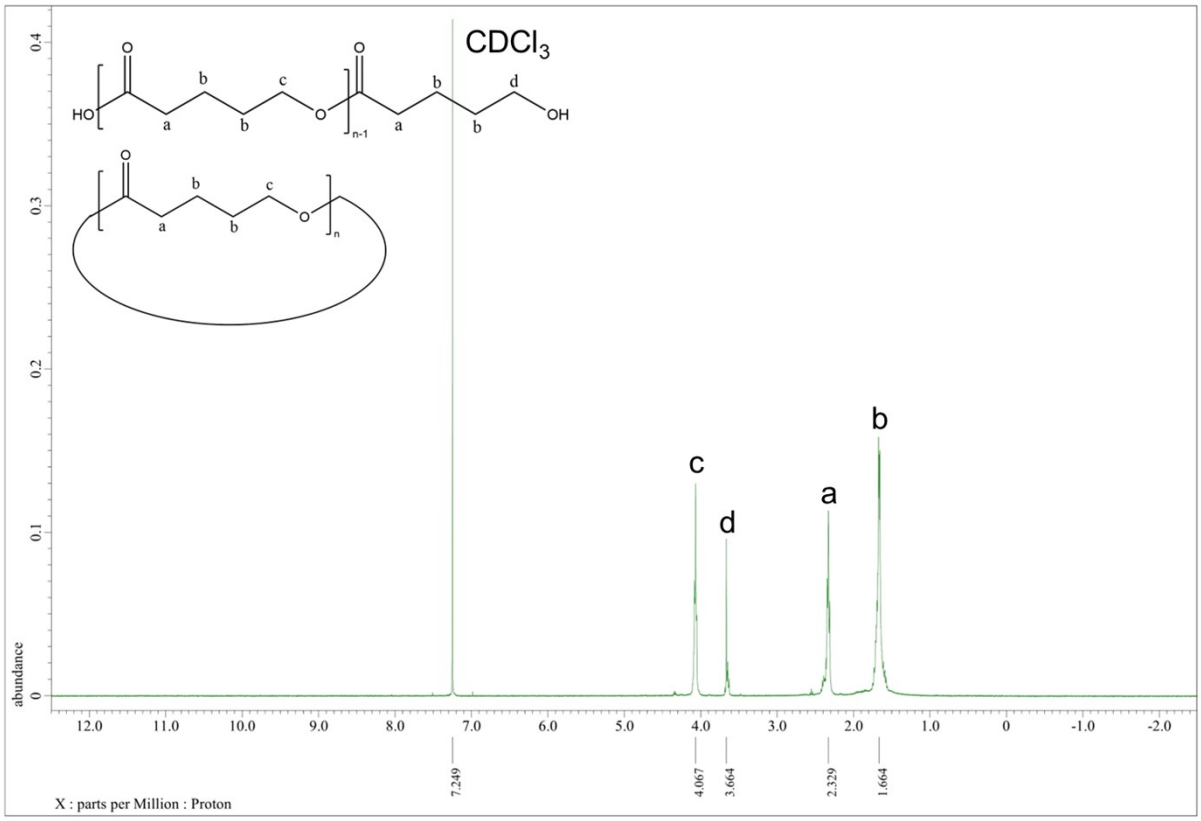

Figure S21. [1]H NMR spectrum for PVL (Table 2, entry 11).

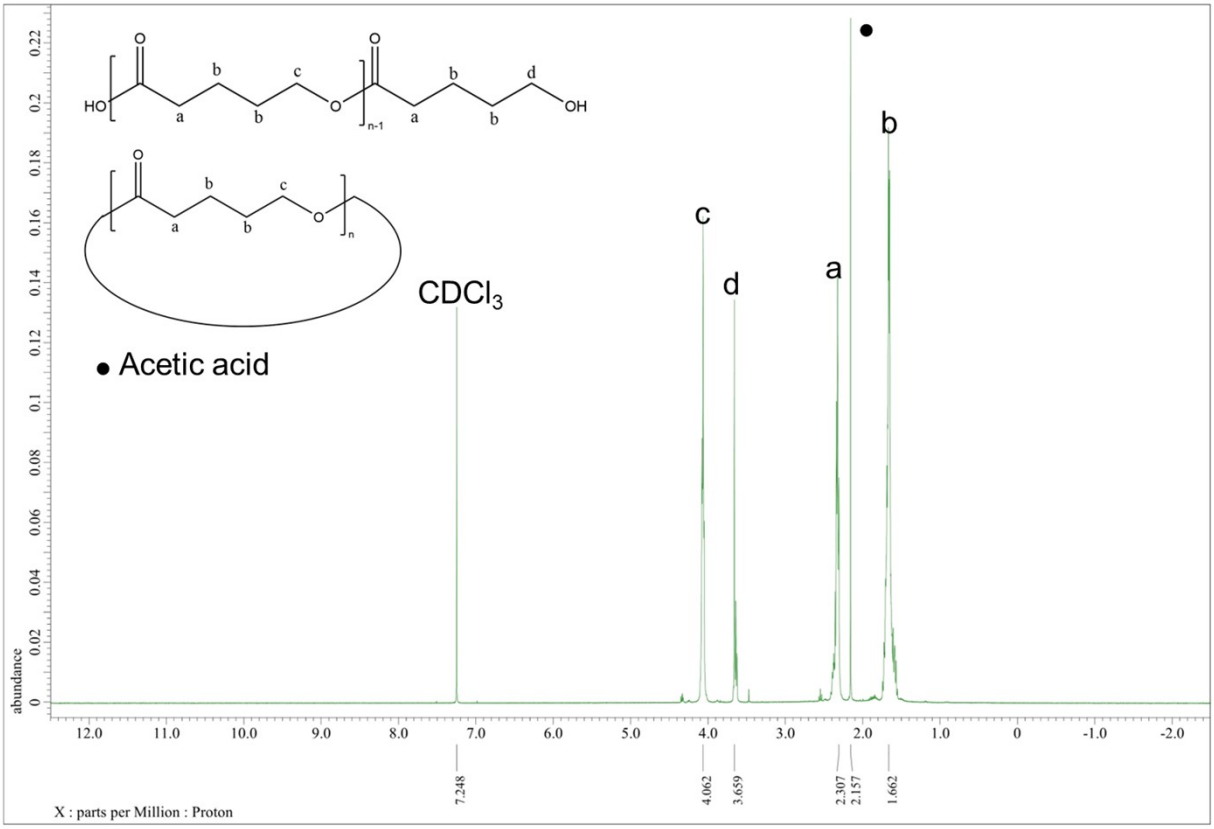

Figure S22. ^{1}H NMR spectrum for PVL (Table 2, entry 12).

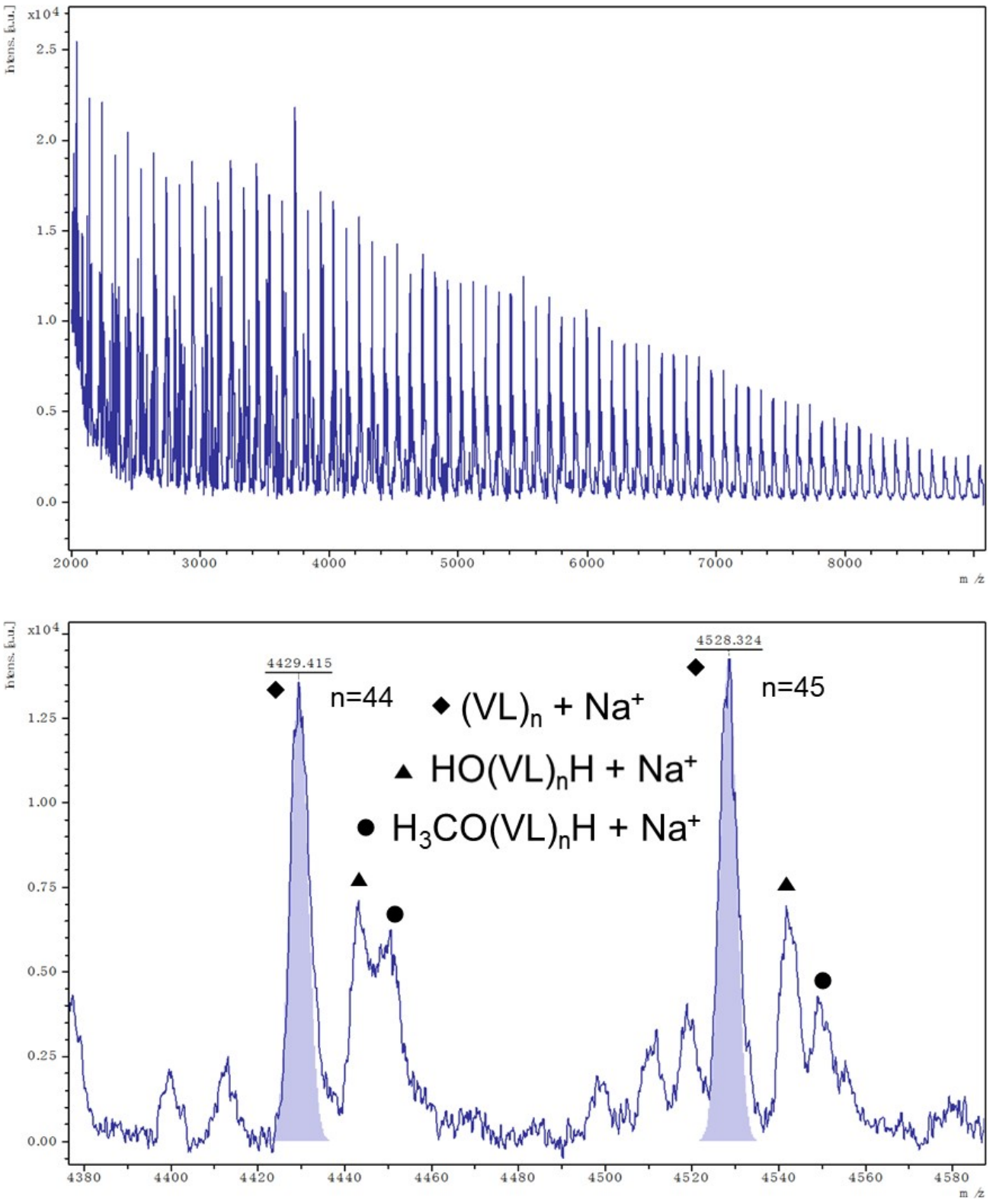

Figure S23. MALDI-TOF mass spectrum of PVL (Table 2, entry 2).

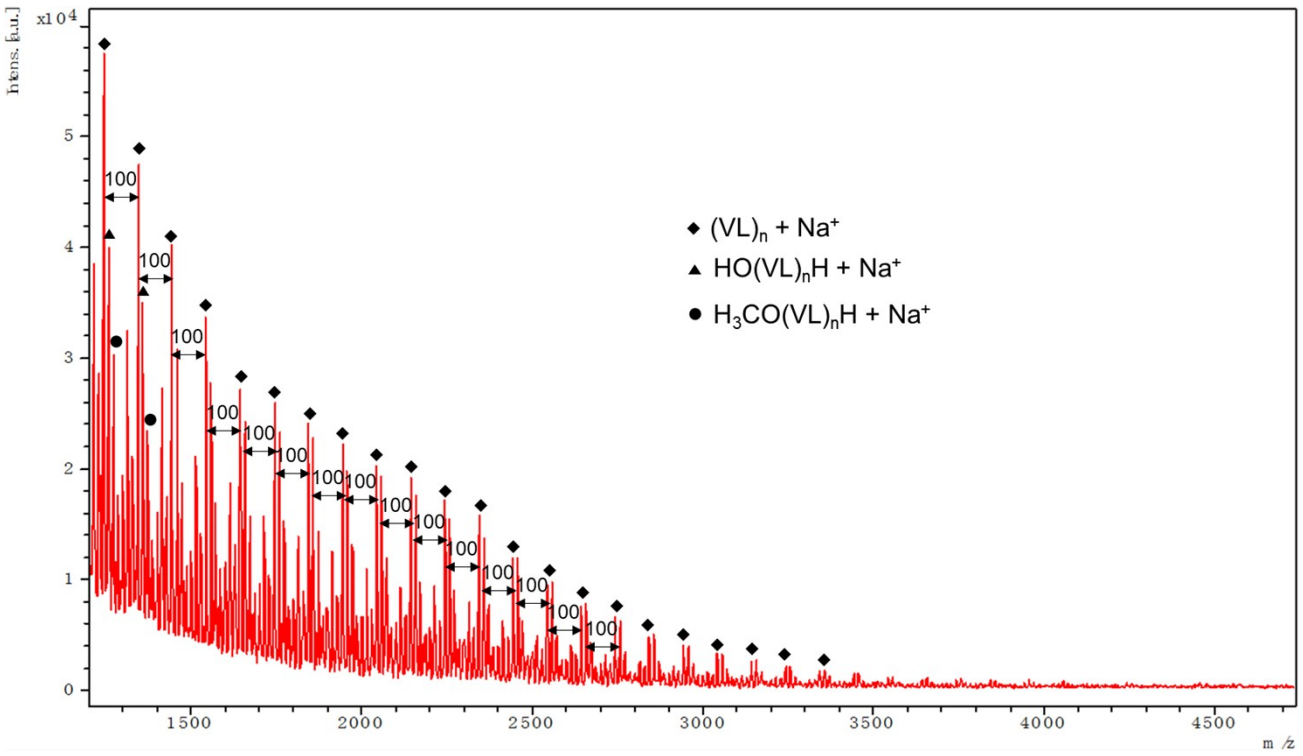

Figure S24. MALDI-TOF mass spectrum of PVL (Table 2, entry 3).

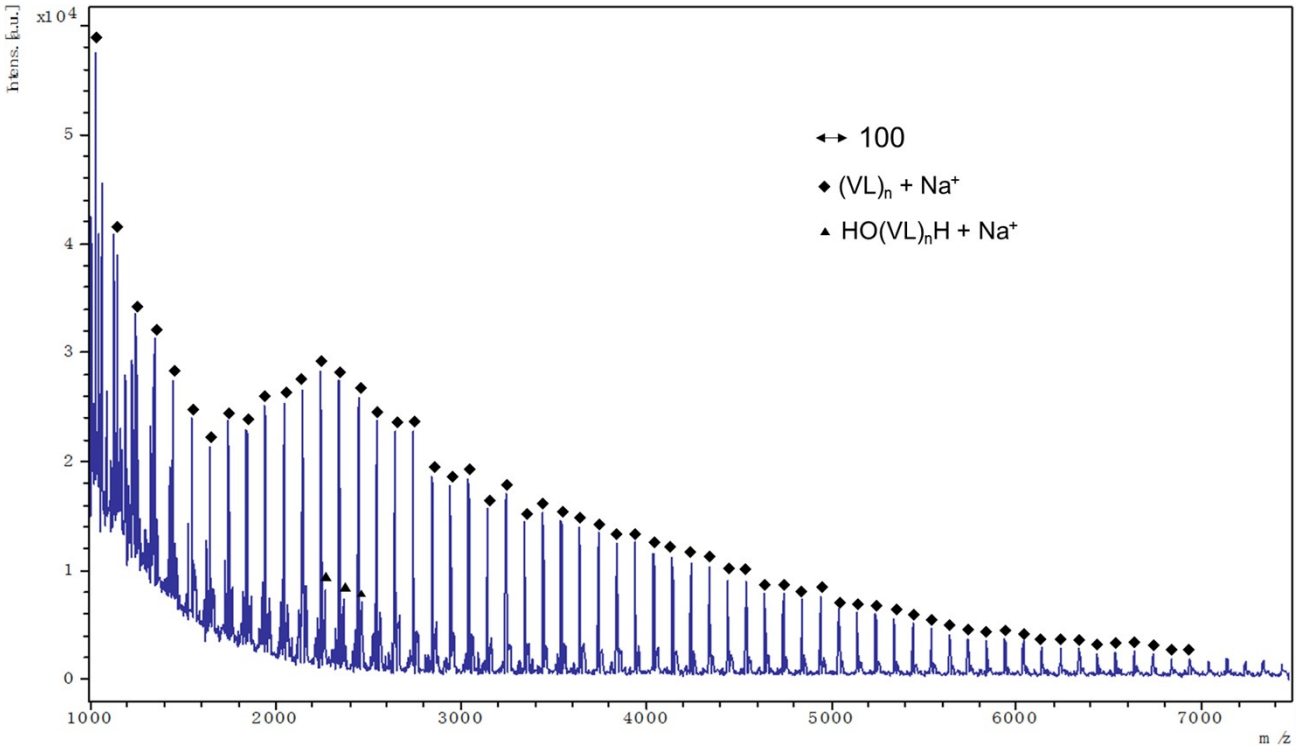

Figure S25. MALDI-TOF mass spectrum of PVL (Table 2, entry 4).

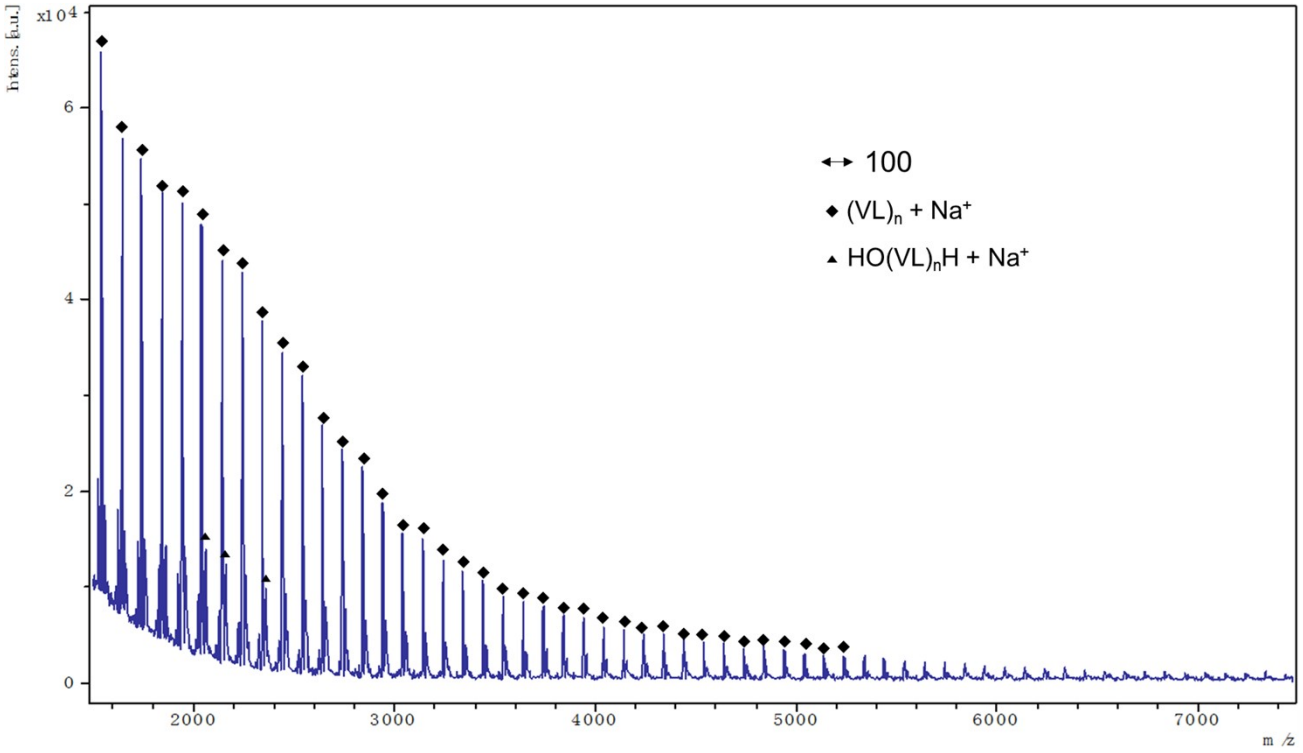

Figure S26. MALDI-TOF mass spectrum of PVL (Table 2, entry 5).

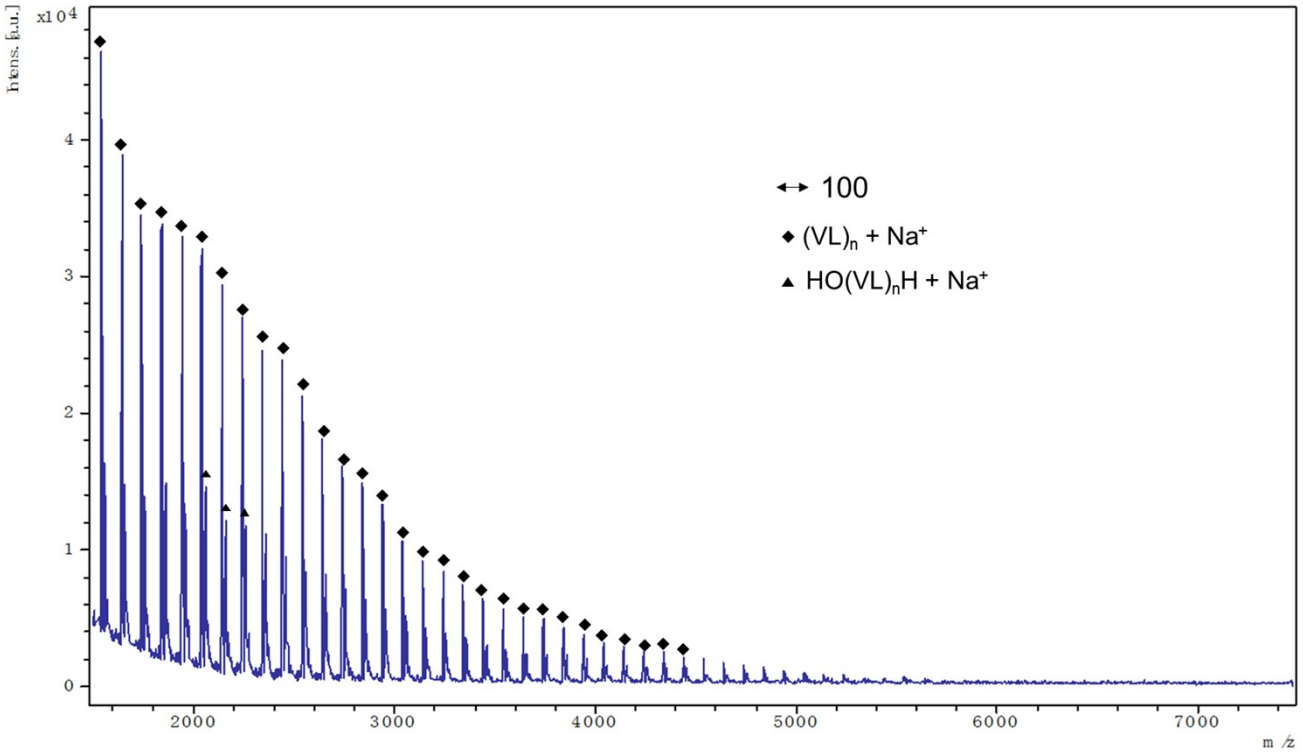

Figure S27. MALDI-TOF mass spectrum of PVL (Table 2, entry 6).

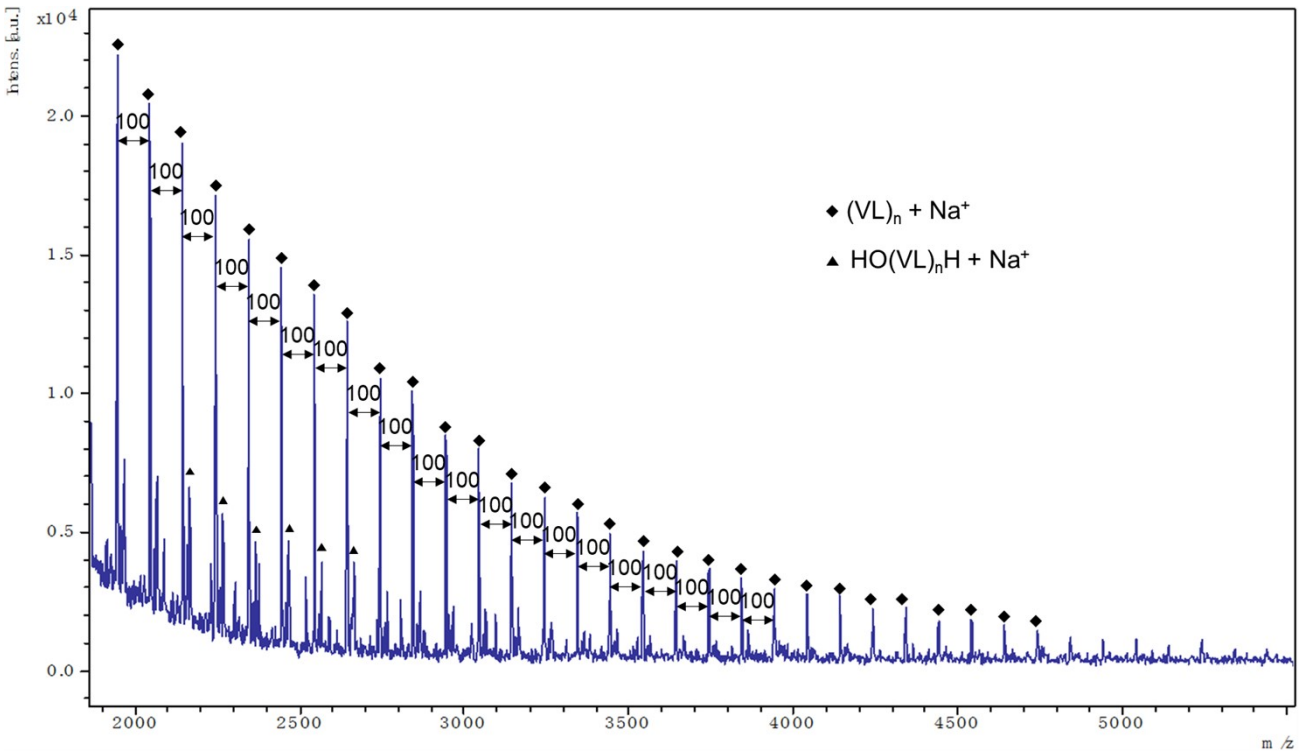

Figure S28. MALDI-TOF mass spectrum of PVL (Table 2, entry 7).

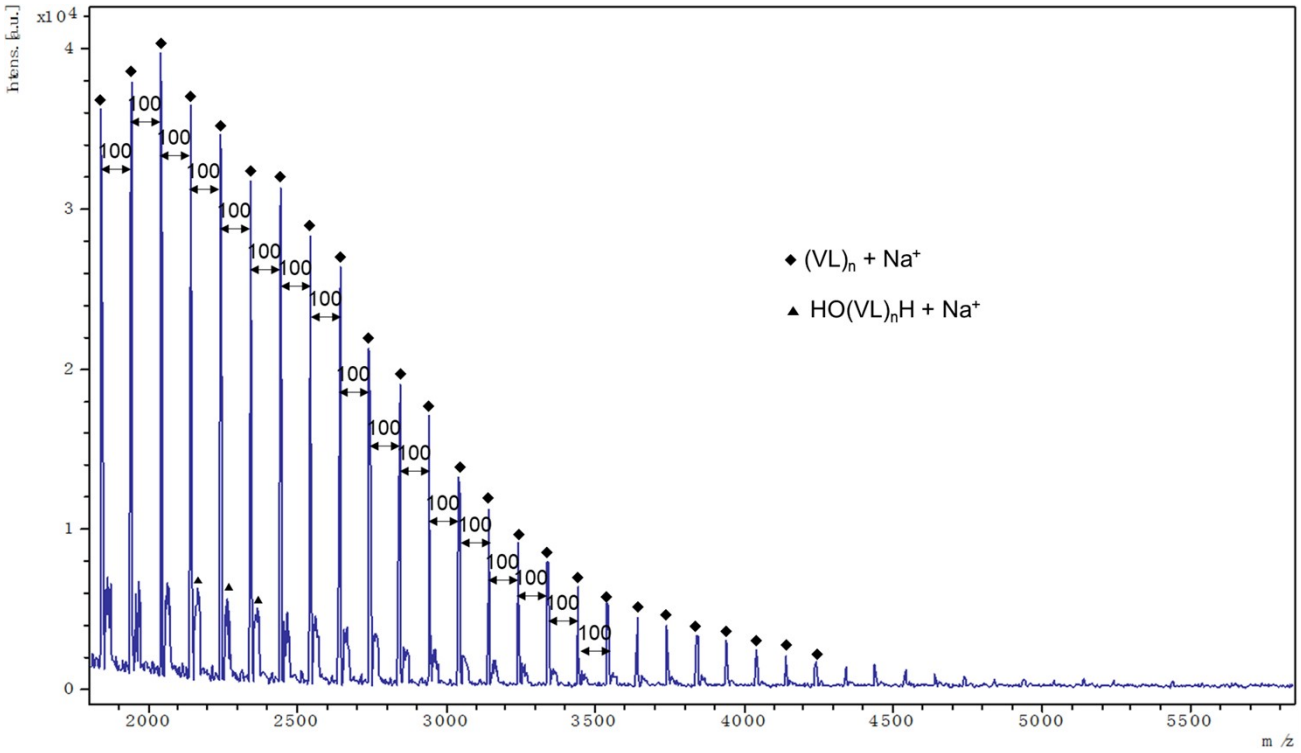

Figure S29. MALDI-TOF mass spectrum of PVL (Table 2, entry 8).

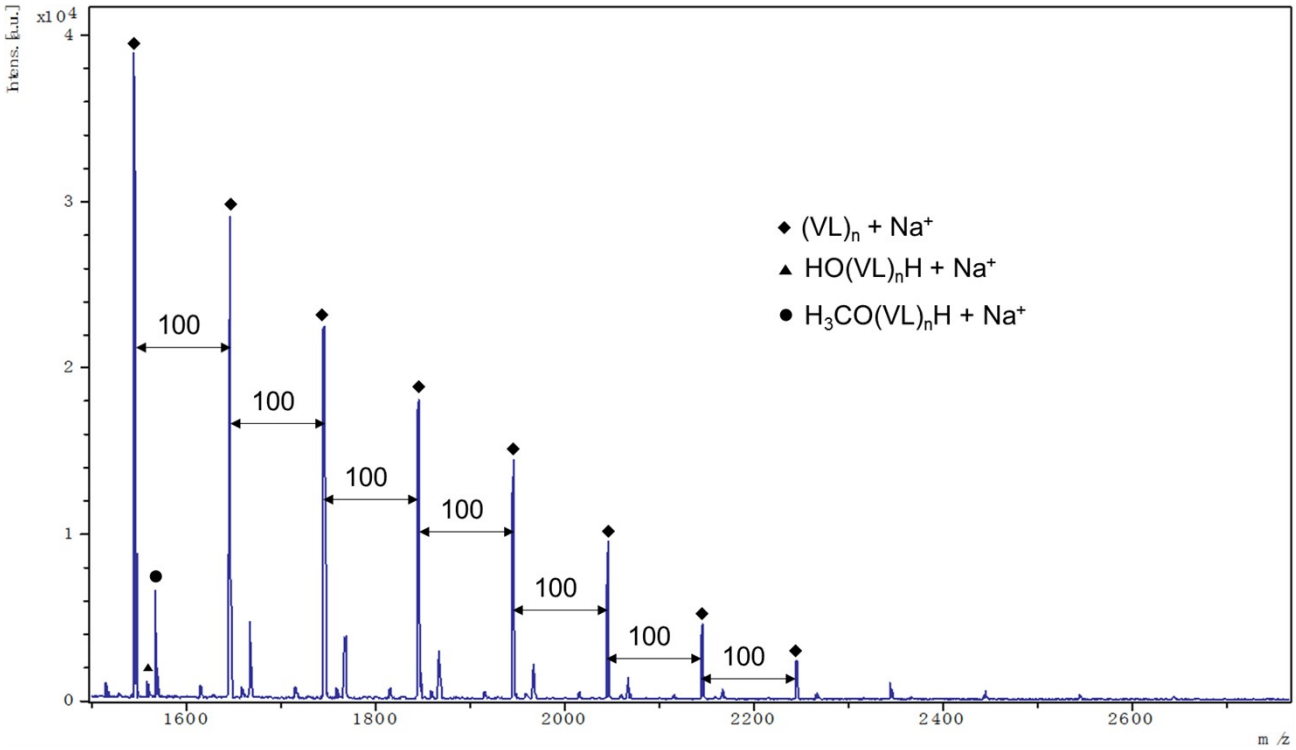

Figure S30. MALDI-TOF mass spectrum of PVL (Table 2, entry 9).

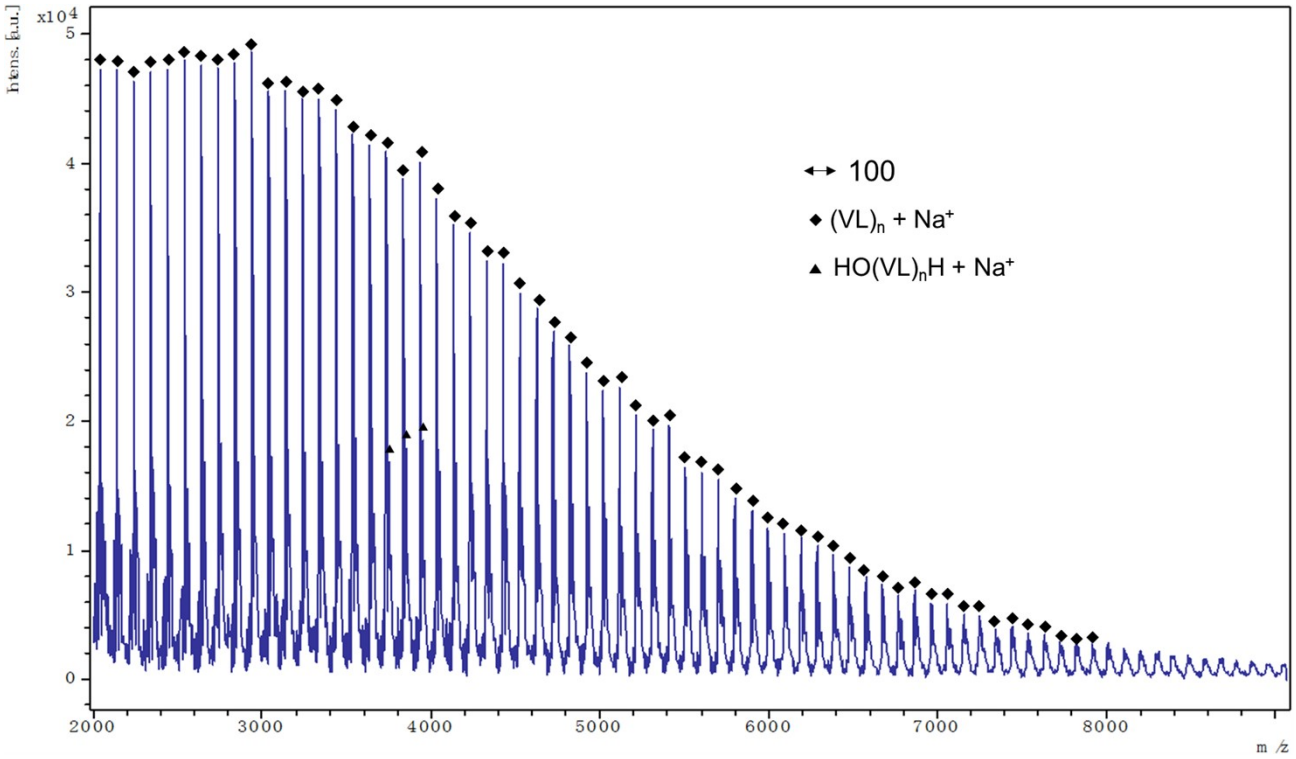

Figure S31. MALDI-TOF mass spectrum of PVL (Table 2, entry 10).

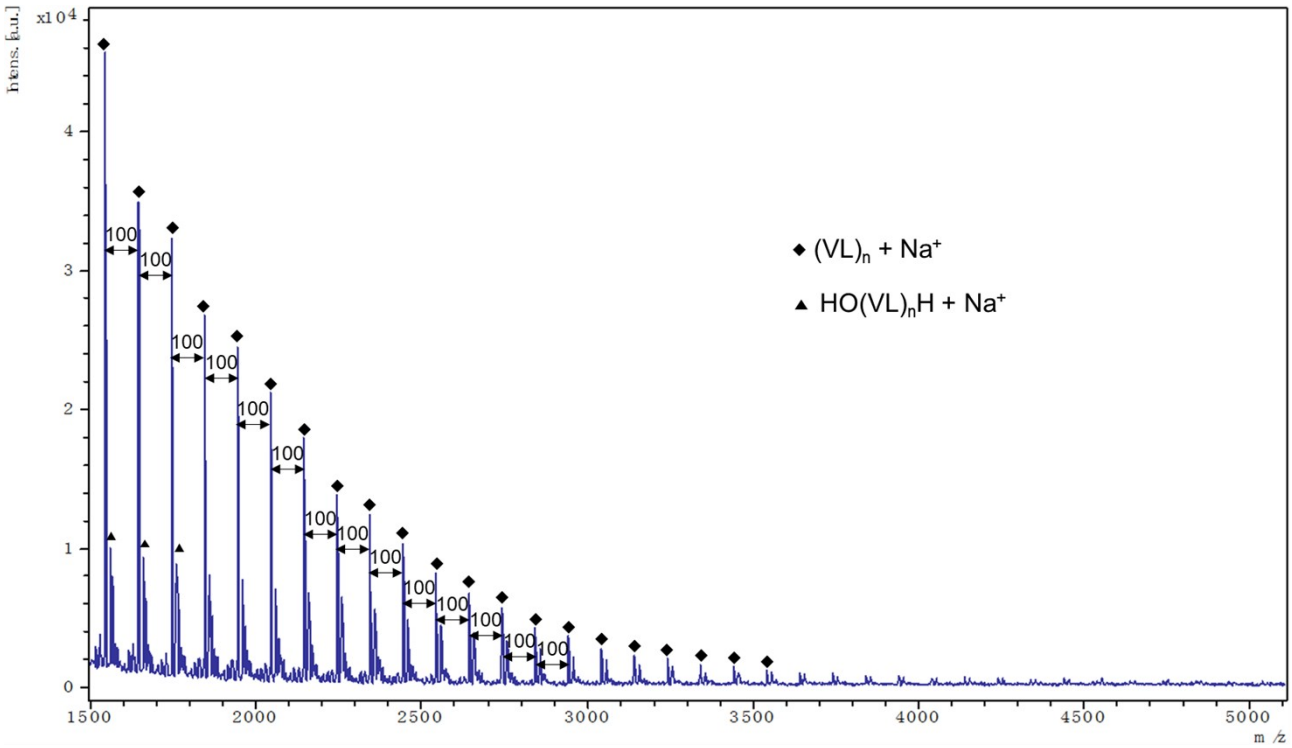

Figure S32. MALDI-TOF mass spectrum of PVL (Table 2, entry 11).

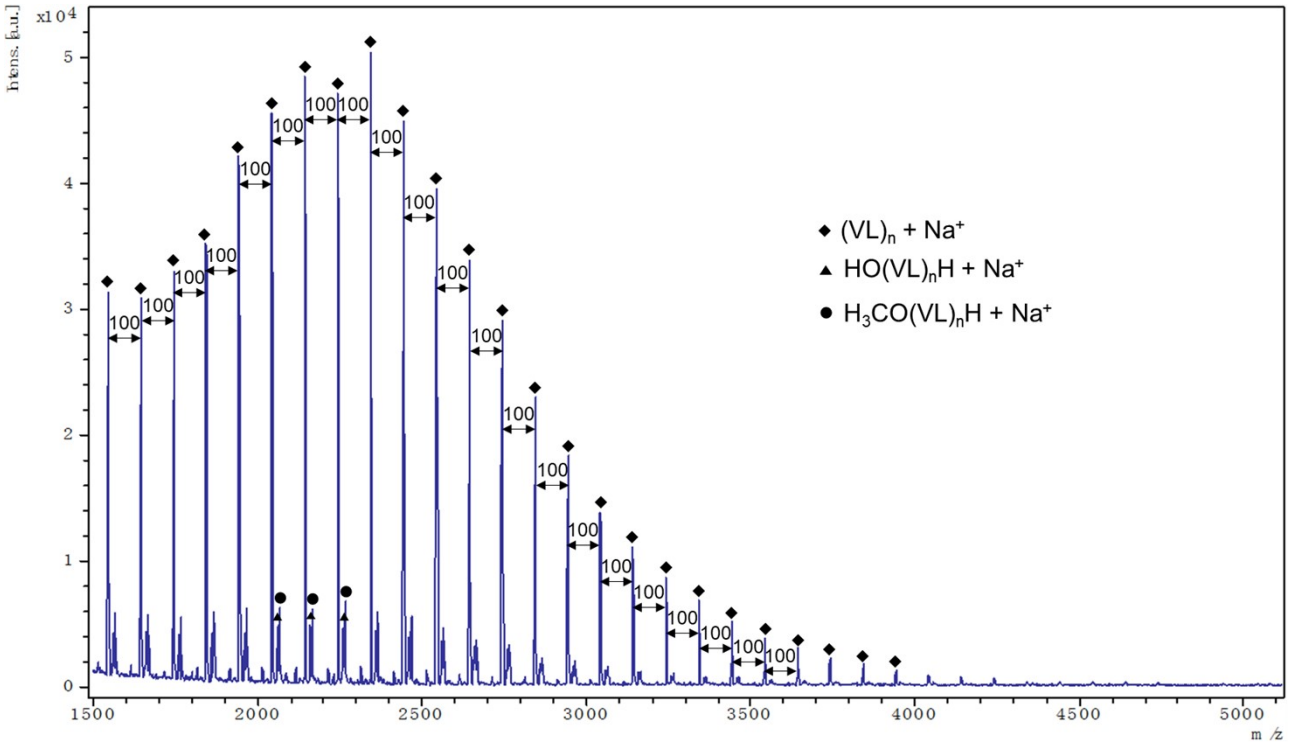

Figure S33. MALDI-TOF mass spectrum of PVL (Table 2, entry 12).

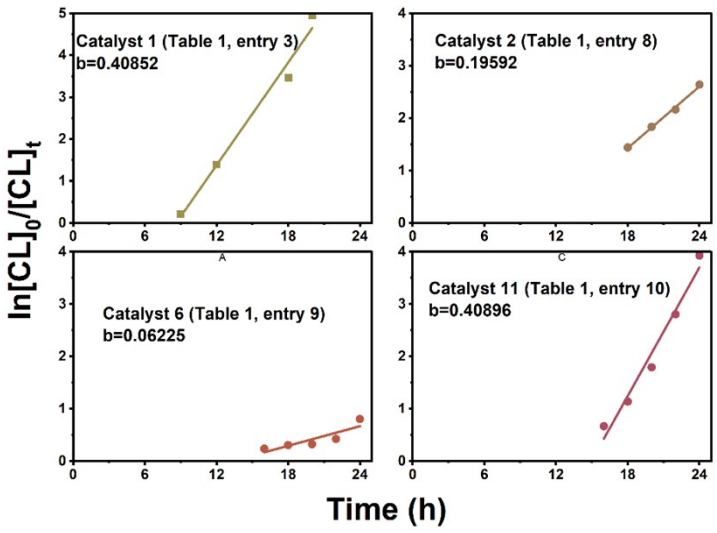

Figure S34. Plot of $\ln[CL]_0/[CL]_t$ *vs*. time for the polymerization of ε-CL (Table 1, entries 3, 8, 9 and 10).

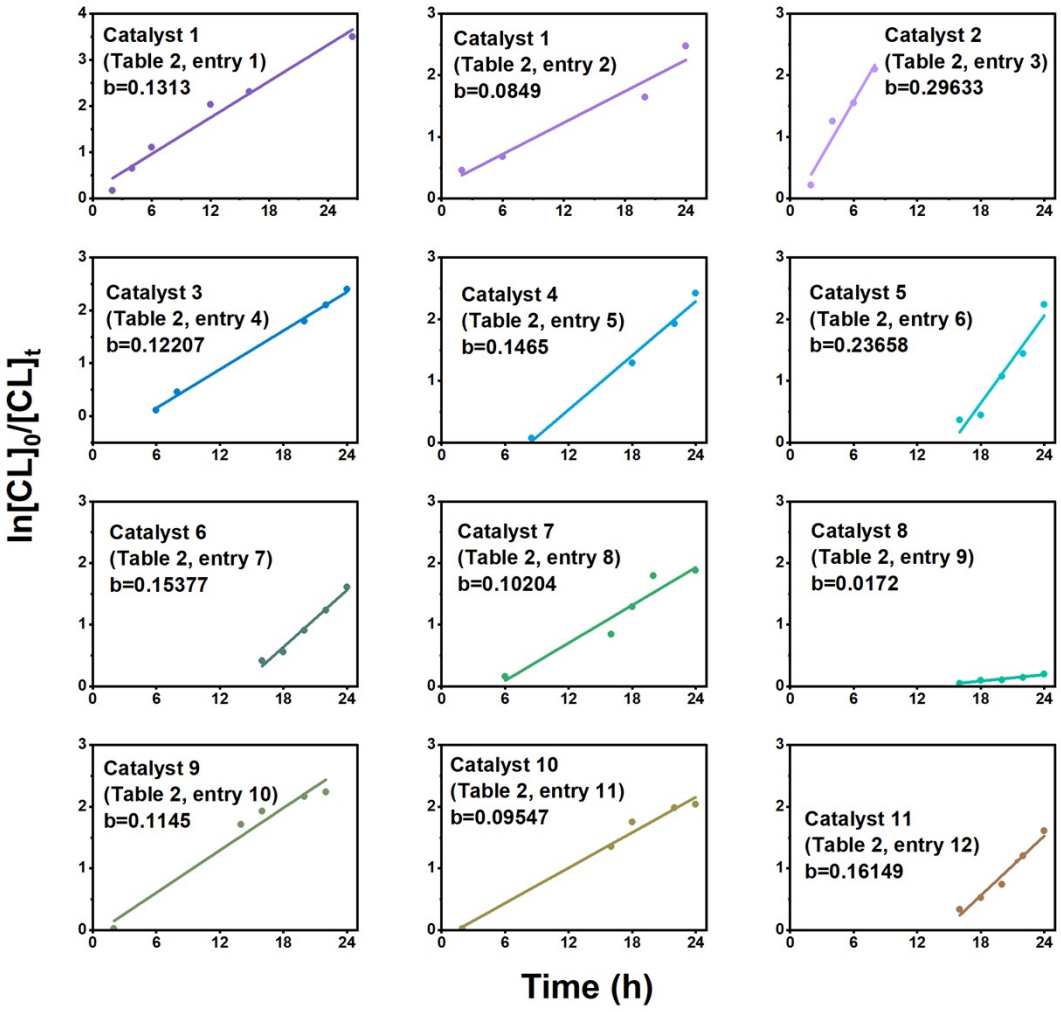

Figure S35. Plot of $\ln[CL]_0/[CL]_t$ *vs*. time for the polymerization of δ-VL (Table 2).

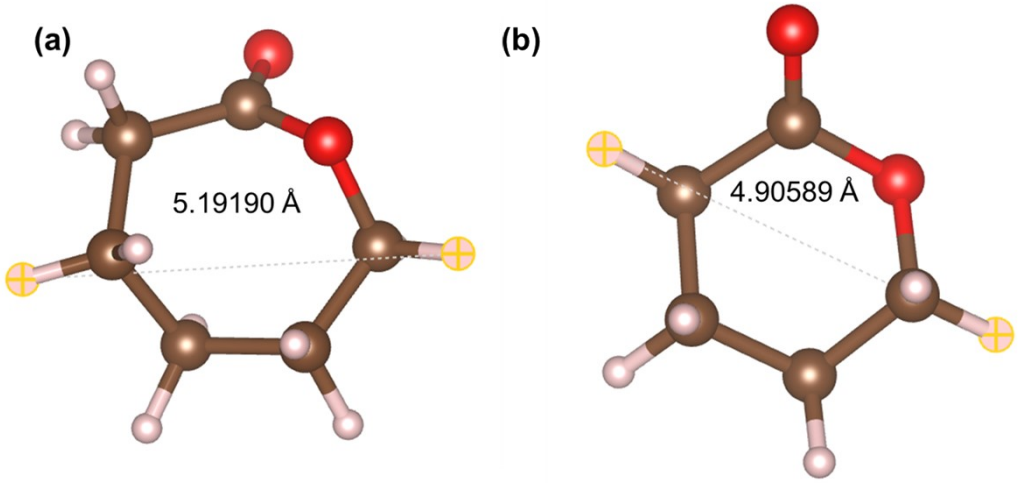

Figure S36. Diameters of the ε-CL and δ-VL monomers.

Table S1. Crystallographic data for structures **1**·DMF and **2**·0.75DMF.

Compound	**1**·DMF	**2**·0.75DMF
Formula	$C_{13}H_9N_2O_4Zn·C_3H_7NO$	$C_{13}H_9N_3O_4Zn·0.75(C_3H_7NO)$
Formula weight (g mol^{-1})	395.69	391.42
Crystal system	Monoclinic	Monoclinic
Space group	*I*2/*a*	$P2_1/c$
a (Å)	16.112(6)	15.01(3)
b (Å)	7.649(3)	7.754(19)
c (Å)	29.100(13)	16.11(3)
α (°)	90	90
β (°)	101.562(5)	109.20(3)
γ (°)	90	90
V (Å^3)	3514(2)	1771(7)
Z	8	4
Temperature (K)	100(2)	100(2)
Wavelength (Å)	0.71073	1.54178
Calculated density (Mg m^{-3})	1.496	1.468
Absorption coefficient (mm^{-1})	1.43	2.21
Transmission factors (max./min.)	0.986, 0.932	1.000, 0.468
Crystal size (mm^3)	0.05 × 0.01 × 0.01	0.18 × 0.06× 0.01
θ_{max} (°)	27.5	57.5
Reflections measured	8779	6600
Unique reflections	3988	2248
Reflections with $F^2 > 2\sigma(F^2)$	3435	1640
R_{int}	0.025	0.170
Number of parameters	215	254
R_1, $wR_2[F^2 > 2\sigma(F^2)]$	0.042, 0.108	0.204, 0.546
GOOF	1.09	1.10
Largest difference peak and hole (e Å^{-3})	0.43, –0.47	2.08, –3.34

Table S2. Crystallographic data for structures **3**·2EtOH, **4**·2DMF and **5**·2DMA.

Compound	**3**·2EtOH	**4**·2DMF	**5**·2DMA
Formula	$C_{28}H_{21}Co_2N_7O_{10}$·2($C_2H_6O$)	$C_{20}H_{15}CoN_3O_4$·2(C_3H_7NO)	$C_{18}H_{13}CoN_5O_4$·2(C_4H_9NO)
Formula weight (g mol^{-1})	825.51	566.47	596.51
Crystal system	Monoclinic	Monoclinic	Monoclinic
Space group	*C*2/*c*	$P2_1/c$	$P2_1/c$
a (Å)	20.5321(19)	13.726(13)	13.20(2)
b (Å)	9.8581(9)	16.881(14)	16.71(2)
c (Å)	18.1007(17)	14.234(13)	14.11(2)
α (°)	90	90	90
β (°)	109.2702(13)	104.396(19)	104.24(3)
γ (°)	90	90	90
V (Å^3)	3458.4(6)	3195(5)	3017(7)
Z	4	4	4
Temperature (K)	150(2)	100(2)	100(2)
Wavelength (Å)	0.71073	0.71073	0.71073
Calculated density (Mg m^{-3})	1.585	1.178	1.313
Absorption coefficient (mm^{-1})	1.03	0.58	0.62
Transmission factors (max./min.)	0.931, 0.610	0.646, 1.000	0.964, 0.941
Crystal size (mm^3)	0.53 × 0.19 × 0.07	0.40 × 0.08 × 0.08	0.10 × 0.09 × 0.06
θ_{max} (°)	28.2	28.0	27.5
Reflections measured	16932	16336	13115
Unique reflections	4235	7669	6401
Reflections with $F^2 > 2\sigma(F^2)$	3213	5861	4462
R_{int}	0.033	0.046	0.046
Number of parameters	319	428	290
R_1, $wR_2[F^2 > 2\sigma(F^2)]$	0.050, 0.159	0.164, 0.451	0.106, 0.337
GOOF	1.05	1.07	1.12
Largest difference peak and hole (e Å^{-3})	0.89, –0.79	2.81, –1.07	1.03, –0.81

Table S3. Crystallographic data for structures **6**·2DMA, **7**·6DMF and **8**·2.5DMF.

Compound	**6**·2DMA	**7**·6DMF	**8**·2.5DMF
Formula	$C_{18}H_{13}MnN_3O_4·2(C_4H_9NO)$	$C_{23}H_{15}MnN_3O_4·6(C_3H_7NO)$	$C_{18}H_{13}MnN_5O_4·2.5(C_3H_7NO)$
Formula weight (g mol^{-1})	564.50	890.88	601.01
Crystal system	Orthorhombic	Monoclinic	Monoclinic
Space group	*Pbam*	$P2_1/c$	$P2_1/c$
a (Å)	14.103(2)	13.880(6)	13.583(6)
b (Å)	17.021(3)	17.016(7)	16.964(8)
c (Å)	11.6095(18)	14.142(9)	14.247(7)
α (°)	90	90	90
β (°)	90	104.79(4)	108.880(5)
γ (°)	90	90	90
V (Å^3)	2786.8(8)	3229(3)	3106(3)
Z	4	4	4
Temperature (K)	150(2)	150(2)	150(2)
Wavelength (Å)	0.71073	0.71073	0.71073
Calculated density (Mg m^{-3})	1.345	1.758	1.285
Absorption coefficient (mm^{-1})	0.52	0.50	0.48
Transmission factors (max./min.)	0.800, 0.647	0.797, 0.717	0.932, 0.741
Crystal size (mm^3)	0.92 × 0.47 × 0.45	0.72 × 0.52 × 0.48	0.67 × 0.17 × 0.15
θ_{max} (°)	30.6	28.5	25.6
Reflections measured	26766	22679	22188
Unique reflections	4437	7901	5731
Reflections with $F^2 > 2\sigma(F^2)$	3675	3712	3579
R_{int}	0.059	0.117	0.089
Number of parameters	188	300	253
R_1, $wR_2[F^2 > 2\sigma(F^2)]$	0.101, 0.253	0.171, 0.421	0.097, 0.308
GOOF	1.08	1.13	1.05
Largest difference peak and hole (e Å^{-3})	1.66, –1.25	5.17, –1.43	1.75, –0.47

Table S4. Crystallographic data for structures **9**·3DMF, **10**·4.5DMF and **11**.

Compound	**9**·3DMF	**10**·4.5DMF	**11**
Formula	$C_{18}H_{13}CdN_4O_4 \cdot 3(C_3H_7NO)$	$C_{20}H_{15}CdN_3O_4 \cdot 4.5(C_3H_7NO)$	$C_{16}H_{16}CdN_4O_5$
Formula weight (g mol^{-1})	667.00	802.68	456.73
Crystal system	Orthorhombic	Monoclinic	Triclinic
Space group	$P2_12_12$	$P2_1/c$	$P\bar{1}$
a (Å)	14.0579(14)	13.9198(9)	8.1035(15)
b (Å)	17.2541(17)	14.1580(7)	8.1227(15)
c (Å)	11.6948(12)	17.2222(9)	13.739(3)
α (°)	90	90	89.277(3)
β (°)	90	108.982(6)	84.236(3)
γ (°)	90	90	77.887(3)
V (Å^3)	2836.6(5)	3209.5(3)	879.7(3)
Z	4	4	2
Temperature (K)	150(2)	107.8(3)	150(2)
Wavelength (Å)	0.71073	0.71073	0.71073
Calculated density (Mg m^{-3})	1.562	1.661	1.724
Absorption coefficient (mm^{-1})	0.83	0.75	1.28
Transmission factors (max./min.)	0.968, 0.673	1.00, 0.270	0.916, 0.767
Crystal size (mm^3)	0.52 × 0.08 × 0.04	0.84 × 0.09 × 0.09	0.22 × 0.19 × 0.07
θ_{max} (°)	28.4	33.1	28.4
Reflections measured	24395	40289	17030
Unique reflections	7074	14572	4354
Reflections with $F^2 > 2\sigma(F^2)$	5318	14081	3727
R_{int}	0.066	0.145	0.053
Number of parameters	273	255	244
R_1, $wR_2[F^2 > 2\sigma(F^2)]$	0.067, 0.164	0.078, 0.196	0.033, 0.074
GOOF	1.04	1.13	1.06
Largest difference peak and hole (e Å^{-3})	4.53, –0.77	4.77, –3.35	1.06, –0.78

References

1 CYLview, 1.0b; Legault, C. Y., Université de Sherbrooke, 2009 (http://www.cylview.org).

2 K. Momma and F. Izumi, *J. Appl. Crystallogr.*, 2011, **44**, 1272-1276.

3 G. M. Sheldrick, *Acta Crystallogr*. 2008, **A64**, 112-122.

4 G.M. Sheldrick, *Acta Cryst*. 2015, **A71,** 3-8.

5 G.M. Sheldrick, *Acta Cryst*. 2015, **C71,** 3-8.

6 A. L. Spek, *Acta Crystallogr*. 2015, **C71**, 9-18.

7 P.v.d. Sluis and A.L. Spek, *Acta Cryst*allogr. 1990, **A46**, 194-201.